Mechanism of Abnormal Surface Subsidence Induced by Fault Instability

Gangyan Zhang (zhanggangyan@tdkcsj.com)
China Coal Research Institute, Beijing

Research

Keywords: abnormal subsidence, faults slip, mining in hanging wall and footwall, stepped subsidence, blocking effect

Posted Date: December 17th, 2020

DOI: https://doi.org/10.21203/rs.3.rs-127360/v1

Mechanism of abnormal surface subsidence induced by fault instability

Zhang Gangyan*

Abstract Surface movement and deformation with faults differ significantly from that without faults, which the surface movement and deformation at the fault outcrop generally abnormally increase when a fault occurs in the overlying strata and loses stability as a result of mining. To explore the mechanism of abnormal surface subsidence induced by fault instability due to mining in the hanging wall and footwall, mechanical models for the fault slip and soil cantilevers were separately established. Moreover, based on numerical and similarity simulation experiment, the difficulty degrees of fault instability were compared and analysed during mining in hanging wall and footwall. The research results show that: (1) the abnormal surface subsidence at fault outcrop is caused by fracture of soil mass at the fault outcrop due to the cantilever effect. (2) The fault zone that can be stabilised during mining in the hanging wall is broader than that during mining in the footwall, and a fault remains stable when mining in hanging wall and the surface at fault outcrop is more likely to experience stepped subsidence when mining in the footwall. (3) Fault stability worsens with the growth of the fault dip angle when mining in hanging wall, the fault is certainly subjected to slip and instability when fault dip angle is lower than the internal friction angle of the rock mass within the fault zone and fault stability strengthens with increasing fault dip angle during mining in the footwall. (4) When mining in the footwall, the ratio of shear stress to normal stress at the fault outcrop is about five times that when mining in the hanging wall and the fault is more likely to undergo slip and instability during mining in the footwall. (5) As a natural weak plane in the rock mass, a fault exerts a blocking effect on the transfer of mining-induced stress and overburden movements.

Keywords: abnormal subsidence, faults slip, mining in hanging wall and footwall, stepped subsidence, blocking effect.

1 Introduction

Surface subsidence with faults in the overlying strata greatly differs from that in

✉Zhang Gangyan
Zhang gangyan@tdkcsj.com
1.Mining Research Institute, China Coal Research Institute, Beijing 100013, China;
2. Coal Mining & Designing Department, Tiandi Science & Technology Co., Ltd., Beijing 100013, China

more common geological conditions; in the early 1980s, scholars from the United States found that, when a fault occurs in the overlying strata and mining triggers fault activation, step-like cracks are generated at the fault outcrop (Nelson, 1981). During a survey of surface subsidence in Liege, Belgium, Dumont suggested that the surface subsidence mainly depends on fault dip angle and the position of the working face. After a fault is activated, failure at the fault outcrop will be inevitable (Donnelly, 2014). According to Lloyd (1918), the surface differential subsidence will occur at the fault outcrop due to the mining and the boundary angle generally declines during mining in the hanging wall. Fault dip angle determines the subsidence values found through Briggs' surveys (1929) in Great Britain, the United States, and Australia: when there is a small fault dip angle, the mining-affected area will expand and *vice versa*. Based on regression analysis of the measurements at fault outcrops under the effect of 25 faults around the world, The Mining Research Institute of China Coal Research Institute in Beijing (1981) obtained the step drops formula. By performing field measurements on surface subsidence caused by fault slip, Lee (1965) found that fault is easier to be activated during mining in the footwall and discontinuous subsidence in the two sides of fault outcrop is mainly attributed to a high compressive stress. Fault dip angle determines whether a fault is activated, and it is more likely to be activated at a fault dip angle of 60° to 90°. The infill in fault planes act as the lubricant for, and therefore is conducive to, strata movement (Tyrala, 1975). Wilde and Crook (1984) revealed that the pore water pressure promotes fault activation and fault activation always occurs suddenly but not progressively. If rocks at the fault outcrop are hard to break, the failure range of the surface at fault outcrop will broaden because of the cantilever effect of hard strata (Donnelly, 2000). With the constant improvement of computer technology, numerical simulation is gradually applied to study fault slip. Sainoki (2014) explored the dynamic process of fault slip and the plastic strain in the mining process by numerical simulation.

After the formation of fault, the consolidated soil mass with a certain thickness generally covers the faults due to the wind erosion and relocation during the subsequent long-term geological movement. Mechanical models for fault slip and soil fracture in the effect of cantilever were separately built when mining in the hanging-wall and footwall. On this basis, the mechanism of surface abnormal subsidence induced by the fault slip was analysed in this paper.

2 Establishment of a mechanical model for

fault slip

As a weak plane, a fault breaks the mechanical connection between rock masses in the hanging wall and footwall (Wang *et al*. 1999; Yu *et al*. 2018). During mining in the hanging-wall and footwall, the forces acted on fault plane and the contact modes are shown in Figs. 1(a) and (b).

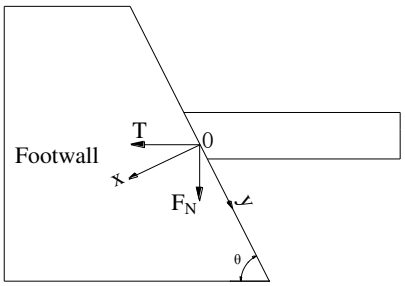

(a) Mining in the hanging-wall

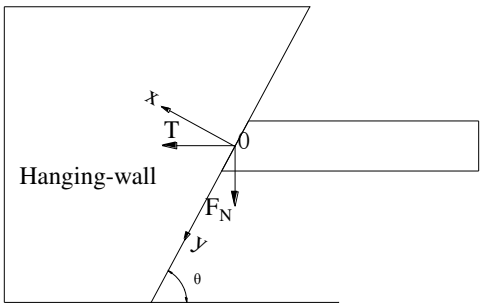

(b) Mining in the footwall

Fig. 1 Free-body diagram during mining in the hanging-wall and footwall

According to mining in the hanging wall, the force at the point O is expressed as:

$$\begin{cases} F_{\mathrm{x}} = F_N \cos\theta + T \sin\theta \\ F_{\mathrm{y}} = F_N \sin\theta - T \cos\theta \end{cases} \tag{1}$$

where, F_{N} and T refer to the vertical and horizontal stress at the contact point, respectively; θ represents the fault dip angle.

The condition that the hanging-wall rock does not slide along the fault plane is displayed as:

$$F_{\mathrm{x}} \tan\varphi \geq \left| F_{\mathrm{y}} \right| \tag{2}$$

where, φ is the internal friction angle of rock mass in the fault zone.

At $F_{\mathrm{y}} \geq 0$, that is

$$\frac{F_N}{T} \geq \cot\theta \tag{3}$$

By substituting Eq. (1) into Eq. (2), we obtain:

$$F_N \sin(\theta - \varphi) \leq T \cos(\theta - \varphi) \tag{4}$$

At $\theta > \varphi$, Eq. (5) can be attained according to Eq. (4):

$$\frac{F_N}{T} \leq \cot(\theta - \varphi) \tag{5}$$

At $\theta < \varphi$, Eq. (6) can be obtained through Eq. (4):

$$\frac{F_N}{T} \geq \cot(\theta - \varphi) \tag{6}$$

At $F_{\mathrm{y}} \leq 0$, that is

$$\frac{F_N}{T} < \cot\theta \tag{7}$$

By substituting Eq. (1) into Eq. (2), it is attained that:

$$F_N \sin(\theta + \varphi) \geq T \cos(\theta + \varphi) \tag{8}$$

φ generally ranges from 38° to 45° (Qian *et al*. 2010) and $\sin(\theta + \varphi) \geq 0$ always exists. Through Eq. (8), we obtain:

$$\frac{F_N}{T} \geq \cot(\theta + \varphi) \tag{9}$$

Thus, the conditions that a fault remains stable when mining in the hanging-wall are attained:

$$\begin{cases} \cot\theta \le \dfrac{F_N}{T} \le \cot(\theta-\varphi) & \theta>\varphi \\ \begin{cases} \dfrac{F_N}{T} > \cot\theta \\ \dfrac{F_N}{T} > \cot(\theta-\varphi) \end{cases} & \theta<\varphi \\ \text{或} \\ \cot(\theta+\varphi) \le \dfrac{F_N}{T} \le \cot\theta \\ \dfrac{F_N}{T} \ge 0 \end{cases} \tag{10}$$

As for the mining in the footwall, the force at point O is resolved into the following components:

$$\begin{cases} F_x = T\sin\theta - F_N\cos\theta \\ F_y = T\cos\theta + F_N\sin\theta \end{cases} \tag{11}$$

The primary condition for faults to maintain stable when mining in the footwall is $F_x > 0$. Otherwise, the footwall rock will separate from the fault plane and the weight of rock in the footwall completely concentrates on the coal pillar in front of the working face, thus compressing the coal pillar, and then triggering fault activation. That is, the following condition needs to be first satisfied to keep a fault stable when mining in the footwall:

$$\frac{F_N}{T} < \tan\theta \tag{12}$$

Moreover, to keep a fault stable, it is still necessary to satisfy Eq. (2). Substituting Eq. (2) into Eq. (11) yields:

$$F_N\sin(\theta+\varphi) \le -T\cos(\theta+\varphi) \tag{13}$$

That is:

$$\frac{F_N}{T} \le -\cot(\theta+\varphi) \tag{14}$$

Thus, the conditions that rock mass remains stable when mining in the footwall are:

$$\begin{cases} \dfrac{F_N}{T} \le -\cot(\theta+\varphi) \\ \dfrac{F_N}{T} < \tan\theta \\ \dfrac{F_N}{T} \ge 0 \end{cases} \tag{15}$$

According to Eqs. (10) and (15), when φ is 45°, the ranges within which the fault can remain stable during mining in the hanging-wall and footwall are respectively shown in Figs. 2(a) and (b).

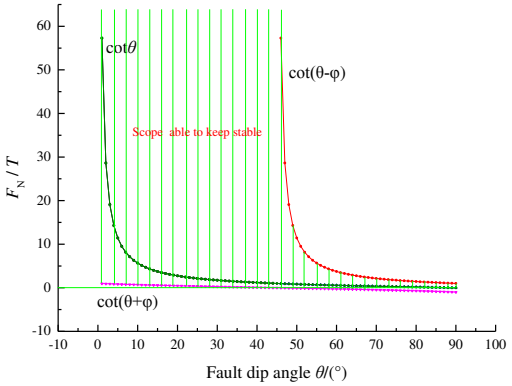

(a) Hanging-wall

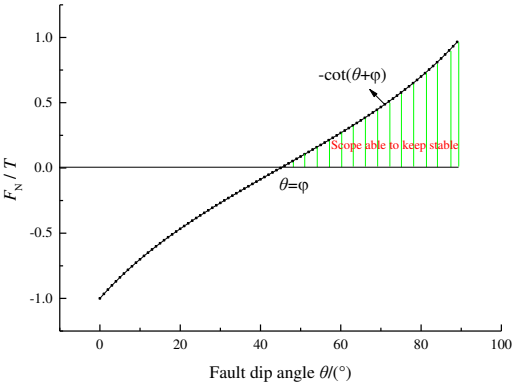

(b) Footwall

Fig. 2 Stable ranges during mining in the hanging-wall and footwall at different fault dip angles θ

It can be seen from Fig. 2 that the stable zone when mining in the hanging-wall is wider than that when mining in the footwall and the

fault is more likely to remain stable during the mining in hanging-wall. Additionally, it can be also found that during mining in the hanging-wall, the fault stability decreases with increasing fault dip angle. When mining in the footwall, the fault is activated at the fault dip angle $\theta < \varphi$ and its stability is enhanced with an increased fault dip angle.

3 Establishment of a mechanical model for fracture of the soil cantilever

With the working face advancing, the soil mass above the goaf is bent and subsides, and the self-weight of the soil mass is directly applied to the rock below. When the working face gradually approaches the fault and results in the mined-wall slipping along fault plane, an approximate cantilever beam structure is formed by the soil mass at fault outcrop due to its long-term consolidation effect and its tensile and shear resistance, as shown in Fig. 3.

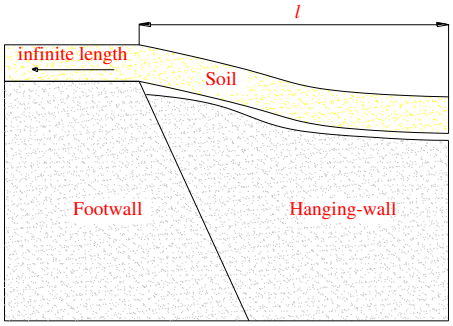

(a) Mining in the hanging-wall

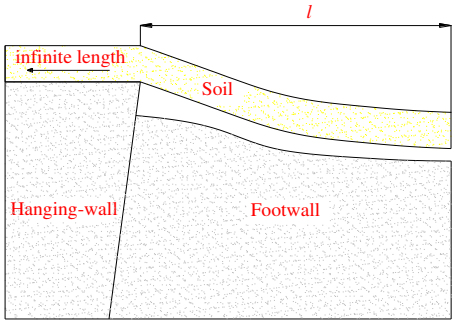

(b) Mining in the footwall

Fig. 3 Cantilever beam formed by the soil mass during mining in the hanging-wall and footwall

The soil mass is bent and subsides downwards under the effect of the gravity. If the bulk density of soil mass is γ, the soil mass bending moment in the cantilever is shown in Fig. 4 (Liu, 2010).

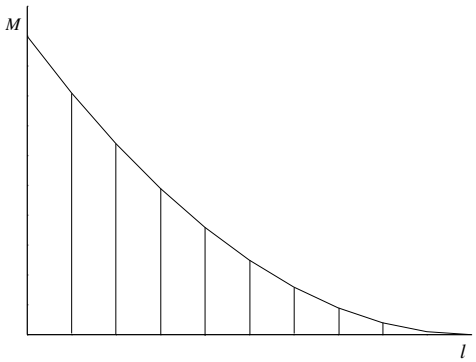

Fig. 4 Bending moment on the soil mass in the cantilever

As shown in Fig. 4, the maximum bending moment of soil mass occurs at the fault outcrop, its value is calculated as:

$$M_{\max} = \frac{1}{2}\gamma l^2 \tag{16}$$

where, γ and l respectively denote the bulk density of the soil mass and the projected length of soil cantilever in the horizontal direction.

A profile is made at the position of soil mass cantilever section, in which the axial direction, height direction and width direction are regarded as x, y, and z separately. The

internal stress on the soil mass under the effect of the applied bending moment is shown in Fig. 5.

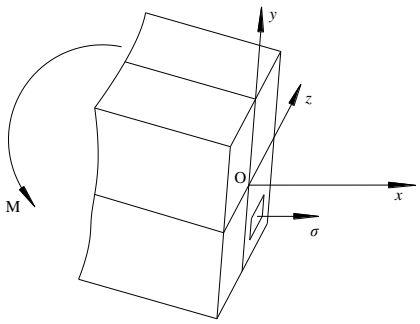

Fig. 5 Internal stress of soil mass cantilever section

The upper and lower parts of soil mass are separately tensed and compressed. The internal stress σ is:

$$\sigma = \frac{My}{I_z} \tag{17}$$

where, M, y, and I_z respectively refer to the bending moment of soil mass cantilever section, the distance to neutral axis and the moment of inertia about the neutral axis.

According to Eqs. (16) and (17), it can be found that after the fault slides, the maximum tensile stress appears on the upper surface of soil mass at fault outcrop due to the cantilever effect. Similar to the rock, the soil mass has a tensile strength that is much lower than the compressive strength (Hou 2010). As a result, some fractures are generated in the upper of soil mass under the effect of the tensile stress and the fractures will run through when it is thin. When the fractures run through the soil, stepped subsidence will occur at the fault outcrop.

4 Numerical simulation analysis of fault slip

Owing to the internal friction angle φ of rock mass in the fault zone is certain, it can be found from Eq. (2) that the ratio of F_x to F_y can determine the fault slip. F_x and F_y separately refer to the normal and shear stress on the rock mass in the fault zone induced by mining activities, which are hard to measure in practice. By using FLAC^{3D}, the change in F_x and F_y is studied during the advance of the working face to the fault. The numerical simulation model is established according to the geological and mining conditions of Jiulong Colliery in Fengfeng Mining Area, Hebei Province, China. The working face advances approximately normal to the strike of the faults, having a strike and dip length of 600 m and 100 m, respectively. Moreover, the mining height, mining depth, and dip angle of coal seams are respectively 5 m, 775 m, and 0° and the fault outcrop is covered by a soil layer with the thickness of 20 m. The normal fault is exposed at the north-west of the working face, with a drop, dip angle, and width of 15 m, 70°, and 5.6 m. The protective coal pillar width between the fault and working face is 50 m. The relative position between fault and working face is shown in Fig. 6.

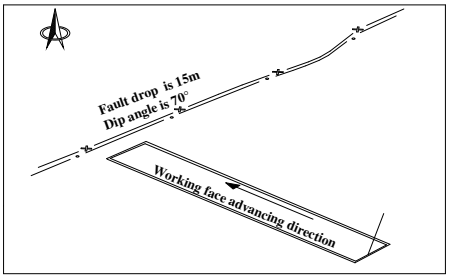

Fig. 6 Relative position of fault and working face

According to the borehole around working face, the lithologic parameters of overlying strata are displayed in Table 1.

Table 1 The overlying strata and their lithologic parameters

Lithology	Thickness /m	Internal friction angle /(°)	Shear modulus /GPa	Bulk modulus /GPa	Cohesion /MPa	Tensile strength /MPa
Soil layer	20	15	0.0038	0.0083	0.3	0.002
Siltstone	250	43	4.3	4.58	6.82	2.35
Sandy mudstone	200	42	3.5	3.56	1.7	2
Mudstone	150	43	6.61	8.89	11.23	4.53
Siltstone	100	43	4.3	4.58	6.82	2.35
Medium-grained sandstone	50	44	0.86	0.81	2.6	1.2
Coal seam	5.32	20	0.13	0.26	0.7	0.9
Fine sandstone	88	39	6.55	8.39	7.59	1.9
Fault zone	5.6	15	0.0038	0.0083	0.3	0.002

The established simulation model for mining in the hanging-wall measures 1729 m × 863 m × 300 m while that for mining in the footwall measures 1490 m × 863 m × 300 m. Except for the upper boundary, other boundaries of models are all fixed. The Mohr-Coulomb failure criterion is adopted in the simulation (Peng, 2007). The simulation models are displayed in Figs. 7(a) and (b).

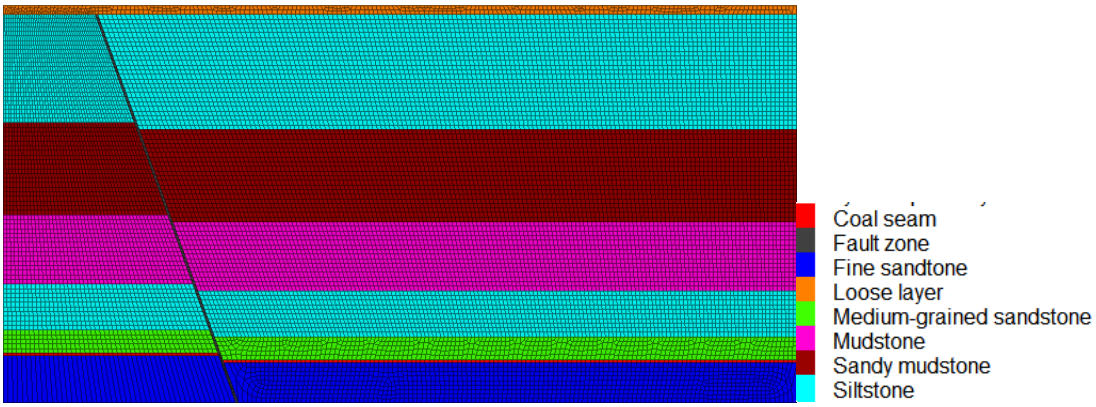

(a) Mining in the hanging-wall

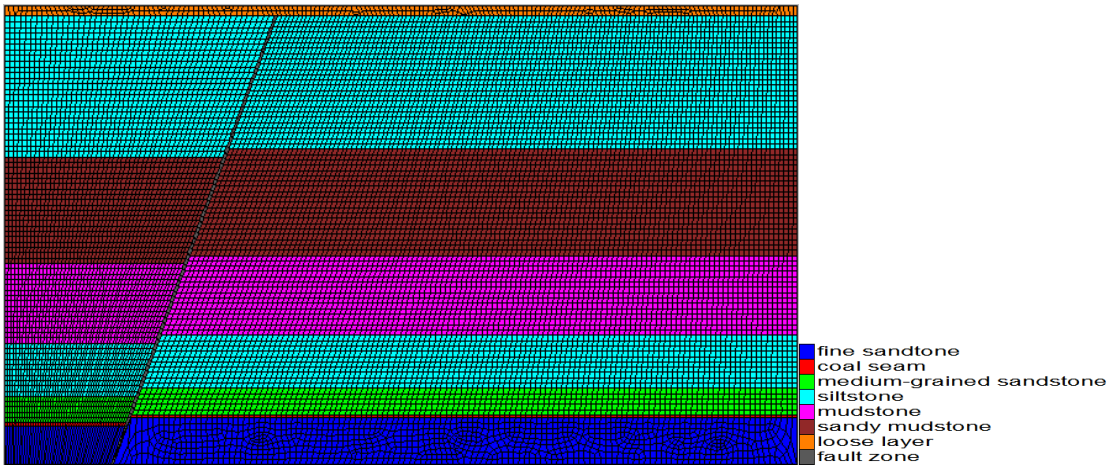

(b) Mining in the footwall

Fig. 7 Simulation models when mining in the hanging-wall and footwall

Only the vertical and horizontal stress of elements can be output through FLAC^{3D}, while the normal and shear stresses of the rock mass in fault zone need to be calculated. A micro-unit is separately taken, as shown in Figs. 8(a) and (b).

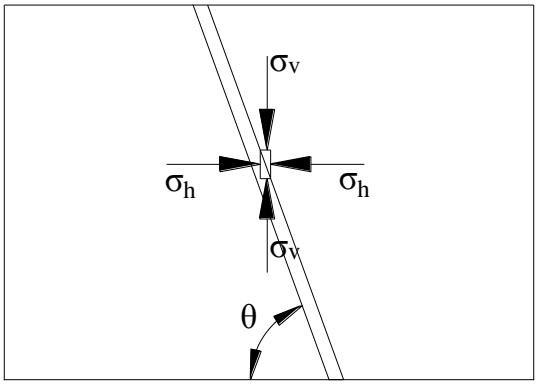

(a) Mining in the hanging-wall

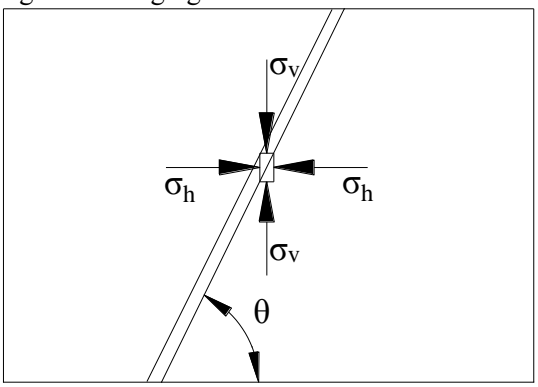

(b) Mining in the footwall

Fig. 8 Diagram of the normal and shear stress calculation when mining in the hanging-wall and footwall

Under effects of the vertical stress σ_v and the horizontal stress σ_h, the normal stress σ and the shear stress τ on the rock mass in fault zone are calculated as follows (Jiao, 2017):

$$\begin{cases} \sigma = \dfrac{1}{2}(\sigma_h + \sigma_v) - \dfrac{1}{2}(\sigma_h - \sigma_v)\cos 2\theta \\ \tau = -\dfrac{1}{2}(\sigma_h - \sigma_v)\sin 2\theta \end{cases} \quad \text{(Mining in the hanging-wall)} \quad (18)$$

$$\begin{cases} \sigma = \sigma_v \cos^2\theta - \sigma_h \sin^2\theta \\ \tau = (\sigma_h + \sigma_v)\sin\theta\cos\theta \end{cases} \quad \text{(Mining in the footwall)} \quad (19)$$

where, σ denotes the normal stress on the rock mass in the fault zone and a negative σ means that the rock mass in the hanging wall imposes a compressive stress on the fault. The larger the negative value is, the higher the normal stress; τ denotes the shear stress on the rock mass in the fault zone and a negative τ represents a shear stress that acts downwards along the fault

plane. The larger the negative is, the higher the shear stress; θ refers to the fault dip angle.

In the process of working face advancing to fault, the ratios of shear stress to normal stress on the rock mass in the fault zone at the fault outcrop when mining in the hanging-wall and footwall with different advancing lengths are shown in Figs. 9(a) and (b).

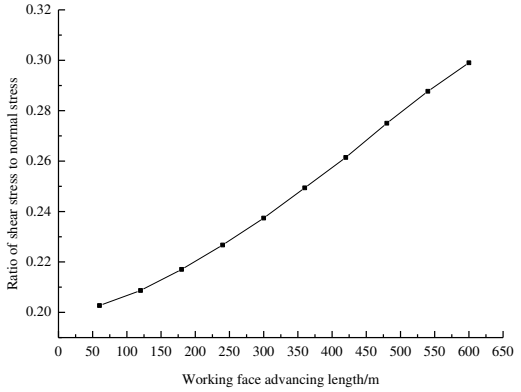

(a) Mining in the hanging-wall

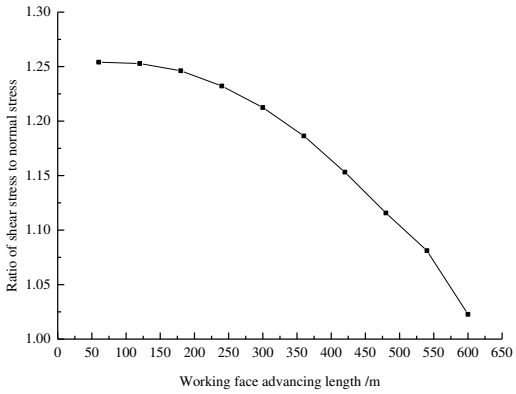

(b) Mining in the footwall

Fig. 9 Ratios of shear stress to normal stress on the rock mass in the fault zone at the fault outcrop in the progress of advancing to the working face to a fault

It can be seen from Fig. 9 that, as the working face advances, the ratio of the shear stress to normal stress on the rock mass in the fault zone when mining in the hanging-wall gradually increases while that when mining in the footwall gradually decreases. During mining in the footwall, the ratio is about five times that during mining in the hanging-wall. As a result, the rock mass in the fault zone when mining in footwall is more likely to experience the slip.

When advancing the working face to a fault, surface subsidence profiles when mining in the hanging-wall and footwall are shown in Figs. 10(a) and (b).

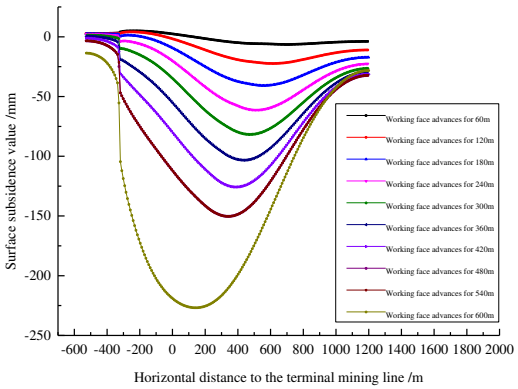

(a) Mining in the hanging-wall

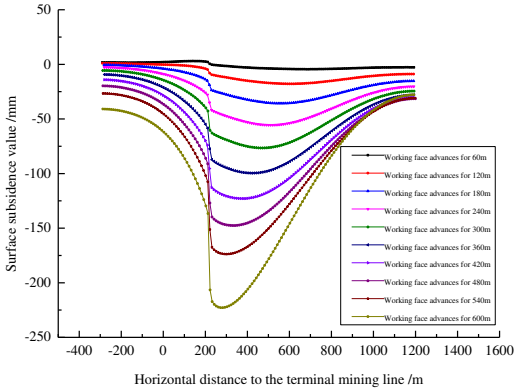

(b) Mining in the footwall

Fig. 10 Surface subsidence when advancing the working face to a fault

As shown in Fig. 10, the value of stepped surface subsidence at the fault outcrop is larger and therefore the faults are more likely to experience slip during mining in the footwall.

5 Similarity simulation analysis of fault slip

To explore the difficulty of fault activation when advancing the working face towards the fault during mining in the hanging-wall and footwall, two similarity models were established according to the geological and mining conditions of Jiulong Colliery in Fengfeng Mining Area. The two models were separately constructed for mining in both the hanging-wall and footwall. The average burial depth of mined coal seams is 775 m. Thus, in view of the stability of similarity models and the experimental effects, the actual thickness of the overlying strata is lowered in proportion while keeping the stratigraphical relationship of overlying strata unchanged. The actual thickness of the adjusted overlying strata is 268 m. According to the experimental conditions and purpose, the geometric similarity constant α_l is 200, the similarity constant for the bulk density α_γ is 1.6, and the similarity constant for strength σ_α is 320. Tabulated ratios of similar materials prepared by the Laboratory of Strata Movement, China University of Mining and Technology, Beijing were applied during the experiment (He, 1991). By taking sand and mica powder as aggregates, gypsum and calcium carbonate as cements, large mica sheets as the sandwich materials and borax as the retarder, the lithological parameters of the overlying strata and ratios of materials of the similarity models for mining in the hanging-wall and footwall are listed in Table 2 according to the actual strength of coal-rock masses and the above three similarity constants (α_l, α_γ, and σ_α).

Table 2 The lithological parameters and ratios of the overlying strata in similarity models when mining in the hanging-wall and footwall

Lithology	Actual thickness /m	Model thickness /mm	Actual bulk density kg/m^3	Bulk density of the model kg/m^3	Actual compressive strength /MPa	Compressive strength of the model /MPa	Ratio (fine sand: mica powder: cement)
Loose layer	8	40	1800	1125	10	0.03	94:4:2(3:7)
Siltstone	76	380	2612	1632.5	81.3	0.25	88:4:8(5:5)
Sandy mudstone	74	370	2350	1468.75	67.5	0.21	89:5:6(5:5)
Mudstone	56	280	2538	1586.25	36	0.11	92:3:5(3:7)
Siltstone	36	180	2612	1632.5	81.3	0.25	88:4:8(5:5)
Medium-grained sandstone	18	90	2570	1606.25	59	0.18	88:4:8(3:7)
Coal seam	5	25	1400	875	29.3	0.09	94:3:3(7:3)
Fault zone	5.6	28	1800	1125	10	0.03	94:4:2(3:7)

The two similarity models are displayed in Figs. 11(a) and (b).

(a) Mining in the hanging-wall

(b) Mining in the footwall

Fig. 11 Similarity models when mining in the hanging wall and footwall

It was attempted to monitor the movement and deformation of overlying strata and the influence of a fault on the mining-induced stress when working face gradually advances to the fault. Measuring points for displacement were set on the surface of models at 100-mm intervals along the horizontal and vertical directions. The movement and deformation of overlying strata were monitored by employing close-range photogrammetry. The stress sensors were distributed in the coal seam floor at 50-mm intervals to monitor the change in advanced abutment pressure in the excavation process.

When mining in the hanging wall, fault slip starts to occur and fractures appear in the rock mass in the fault zone when the included angle of the line connecting the fault outcrop and working face with the horizontal direction is about 51°. As the working face continues to advance, the fractures develop and extend to the surface at the fault outcrop. The relative position between working face and fault when there are fractures in the rock mass within the fault zone is shown in Fig. 12(a). The fractures in the surface at the fault outcrop are displayed in Fig. 13(a). When mining in the footwall, fault starts to slip and some fractures are found in the rock mass within the fault zone when the included angle of the line connecting working face and the fault outcrop with the horizontal direction is 56°. As the working face is advanced, the fractures in the surface at the fault outcrop rapidly expand to form a stepped subsidence profile. The relative position between working face and fault when fractures appear in the rock mass within fault zone is shown in Fig. 12(b) and the stepped subsidence at the fault outcrop is displayed in Fig. 13(b).

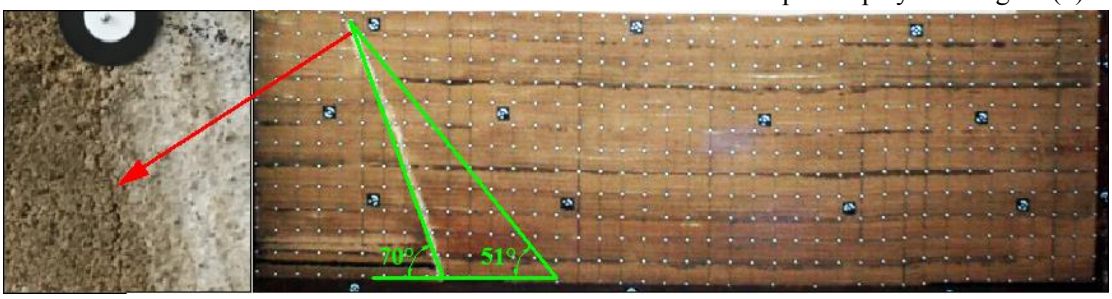

(a) Mining in the hanging-wall

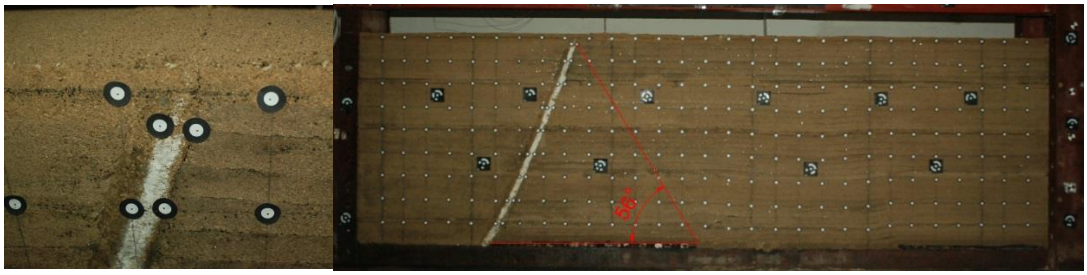

(b) Mining in the footwall

Fig. 12 Relative position of the working face and fault when the fault slips

(a) Mining in the hanging-wall

(b) Mining in the footwall

Fig. 13 Fractures in the surface at fault outcrop when mining is finished

The surface subsidence profiles after completion of mining are shown in Figs. 14(a) and (b).

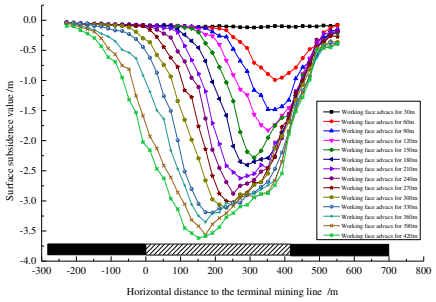

(a) Mining in the hanging-wall

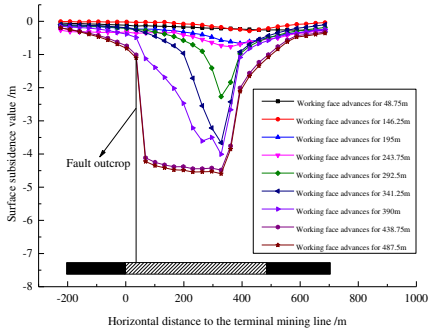

(b) Mining in the footwall

Fig. 14 Surface subsidence profiles when advancing the working face

As shown in Fig. 14, only fractures are generated while no obvious stepped subsidence occurs on the surface at the fault outcrop when mining in the hanging wall. By contrast, significant stepped subsidence is generated on the surface at the fault outcrop when mining in the footwall. Compared with the case of mining in the hanging wall, fault slip is more likely to occur when mining in the footwall, which is consistent with the conclusions obtained through theoretical and numerical simulations.

To monitor the influence of faulting on mining-induced stress during the advance of the working face, the initial pressure on sensors in the floor is set to 0 before excavation of the working face, that is, the *in-situ* stress is regarded as 0. As the working face advances, any positive stress represents a stress above the

in-situ stress; a negative stress is lower than the *in-situ* stress. The difference between the abutment pressure and the *in-situ* stress is defined as the increment of advanced abutment pressure. Changes in the advanced abutment pressure in process of the working face advancing to fault when mining in the hanging-wall and footwall are displayed in Figs. 15(a) and (b).

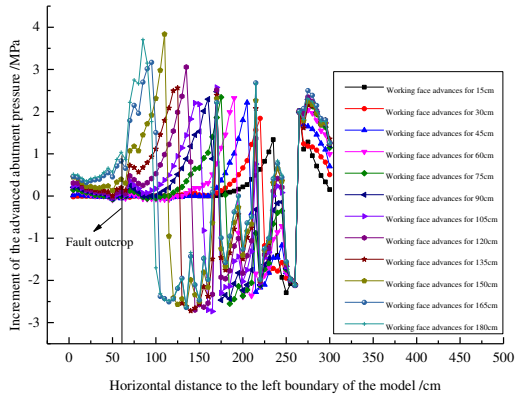

(a) Mining in the hanging-wall

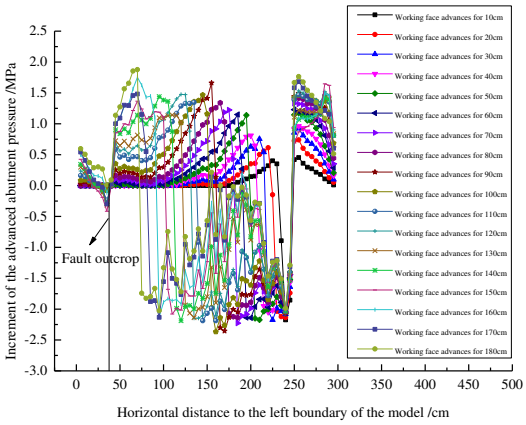

(b) Mining in the footwall

Fig. 15 Changes in advanced abutment pressure when the working face advances to a fault

As shown in Fig. 15, the advanced abutment pressure decreases rapidly at a fault during mining in either the hanging-wall or the footwall: the fault blocks the transfer of advanced abutment pressure.

6 Example verification

The 15233 working face in Jiulong Colliery, Fengfeng Mining Area presents a strike length of 660 m and the dip length of 55 m, with the average burial depth, average mining depth, and coal seam dip angle of 775 m, 5 m, and 8°, respectively. The F37 normal fault was exposed in the northwest of the working face, showing a drop and dip angle of 15 m and 70°, and a fault zone width of 5.6 m. The fault strike is approximately parallel to that of the working face and the protective coal pillar of 17 m wide is reserved. The working face advanced approximately parallel to the strike of the fault when mining in the hanging-wall. According to the angle parameters of Fengfeng mining area, the boundary of the mining-affected zone and the dangerous moving boundary are displayed in Fig. 16.

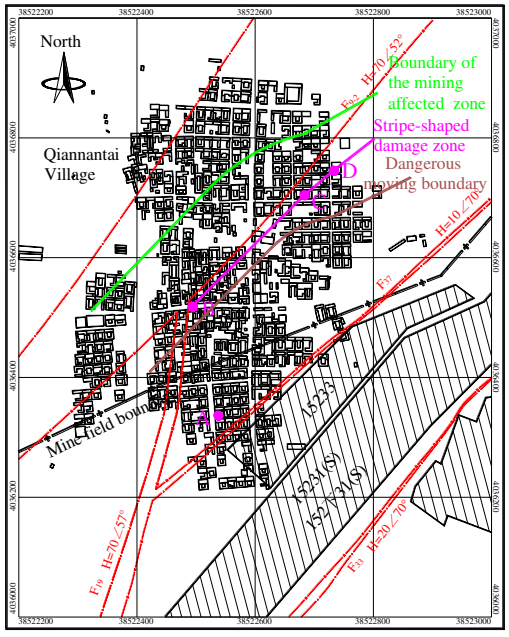

Fig. 16 The boundary of the zone affected by mining and the dangerous moving boundary

When there is no fault, the damage of buildings in Qiannantai villages around the working face should be concentrated on the range within the dangerous moving boundary, however, according to the actual situation on the ground, badly damaged buildings are found beyond the dangerous moving boundary and a strip-shaped damage zone is formed at the fault outcrop (Fig. 16). After mining the 15233 working face, no obvious stepped subsidence was found at the fault outcrop. Nevertheless, buildings at the fault outcrop exhibited grade-IV deformation (Fig. 17).

Fig. 17 Damage to buildings at the fault outcrop

As shown in Fig. 16, the abnormal surface subsidence occurred because the mining caused fault slip and significant movement and deformation at the fault outcrop, thus resulting in severe damage to these buildings.

The No. 2 mining area in the south of the northern wing of Qinghemen Mine, Fuxin mining area, Liaoning Province, China belongs to the Late Jurassic formation of the Mesozoic. A normal fault with the dip angle of 53° is found in the overlying strata which are shown as shale, sandstone, arenaceous shale, and Quaternary alluvium. The working face was mined by a longwall fully-caved coal mining method, with a strike and dip length of 268 m and 234 m. The thickness and dip angle of the coal seam are 1.9 m and 22°. Moreover, the average mining depth was 305 m. The mining occurred in the footwall (Zhang, 1989). The surface subsidence of the main inclined section is shown in Fig. 18.

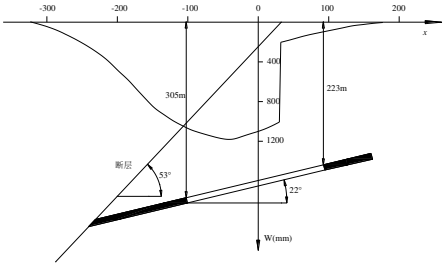

Fig. 18 Surface subsidence profile of the main inclined section in Qinghemen Mine

According to the relative position of the working face and the fault, as well as the measured surface subsidence, it can be found that significant stepped subsidence was generated on the surface at the fault outcrop after completion of the mining work, with the drop of the steps being 500 mm.

7 Conclusion

(1) The abnormal surface subsidence at the fault outcrop occurs because mining causes fault slip, providing room for the deformation and fracturing of the cantilever structure formed by the overlying soil mass at the fault outcrop.

(2) The stable zone during mining in the hanging wall is broader than that during mining in the footwall. Therefore, the fault slip tends to occur, and stepped subsidence is more likely to develop at the fault outcrop when mining in the footwall. With increasing fault dip angle, the stability of the fault is decreased during mining in the hanging wall while it rises during mining in the footwall. Faults are certain to be subject to slip during mining in the footwall when the fault dip angle is lower than the internal friction angle of the rock mass within the fault zone.

(3) The ratio of shear stress to normal stress on the rock mass in the fault zone at the fault outcrop during mining in the footwall is about five times that during mining in the hanging wall. A fault is more likely to slip during mining in the footwall. As a plane of weakness, a fault exhibits a blocking effect on the transfer of mining-induced stress.

References

Nelson W J (1981) Faults and their effect on coal mining in Illinois. Champaign ILL Illinois State Geological Survey.

Donnelly L J (2014) Reactivation of geological faults during mining subsidence from 1859 to 2000 and beyond. Mining Technology 109(3):179-190.

Lloyd W. D (1918) The effect of coal mining on the over-lying rocks and on the surface. Trans. Instn min. Engrs LVII: 74–93.

Briggs H (1929) Mining subsidence. Minutes of the Proceedings 24(1):25-36.

Mining Research Institute of China Coal Research Institute (1981) The law of surface movement and deformation in coal mine and its application. Beijing: Chin Coal Industry Publishing House.

Lee A. J (1965) The effects of faulting on mining subsidence. The Mining Engineer: 735–45.

Tyrala A., Szwedzicka M and Szukalski S (1975) Classification of tectonic faults for investigations on their actions in the process of deformation of the surface[R]. Katowice.

Wilde P. M. and Crook J. M (1984) The significance of abnormal ground movements due to deep coal mining and their effects on large scale surface developments at Warrington New Town. In Proc. Conf. Ground movements and structures, UWIST, Cardiff: 240–247.

Donnelly L J (2000) Fault reactivation induced by mining in the East Midlands. Mercian Geologist 15(1):29-36.

Sainoki A, Mitri H S (2014) Dynamic behavior of mining-induced fault slip. International Journal of Rock Mechanics & Mining Sciences 66(1):19-29.

Wang Mingyang, Zhao Yuetang, Qian Qihu (1999) Studies on mechanism and

quantization of isolation effect of slow angle fault. Chinese Journal of Rock Mechanic and Engineering 18(1):60-64.

Yu Qiuge, Zhang Huaxing, Deng Weinan (2018) Analysis of fault separation generation and its effect on mining zone transferring. Journal of China Coal Society 43(12):3286-3292.

Qian Minggao, Shi Pingwu, Xujialin (2010) Mining pressure and strata control. Xuzhou: China Mining University Press.

Liu Hongwen (2003) Materials mechanics. Beijing: Higher Education Press.

Hou Gongyu (2010) Basic course of Rock Mechanics. Beijing: China Machine Press.

Peng Wenbin (2007) The Finite Element Method of FLAC3D. Beijing: China Machine Press.

Jiao Zhenhua (2017) Research on the evolution law of fault slip and mechanism of coal bumps induced by mining. Beijing: China University of Science and Technology.

He Guoqing (1989) Mining Subsidence. Xuzhou: China Mining University Press.

Figures

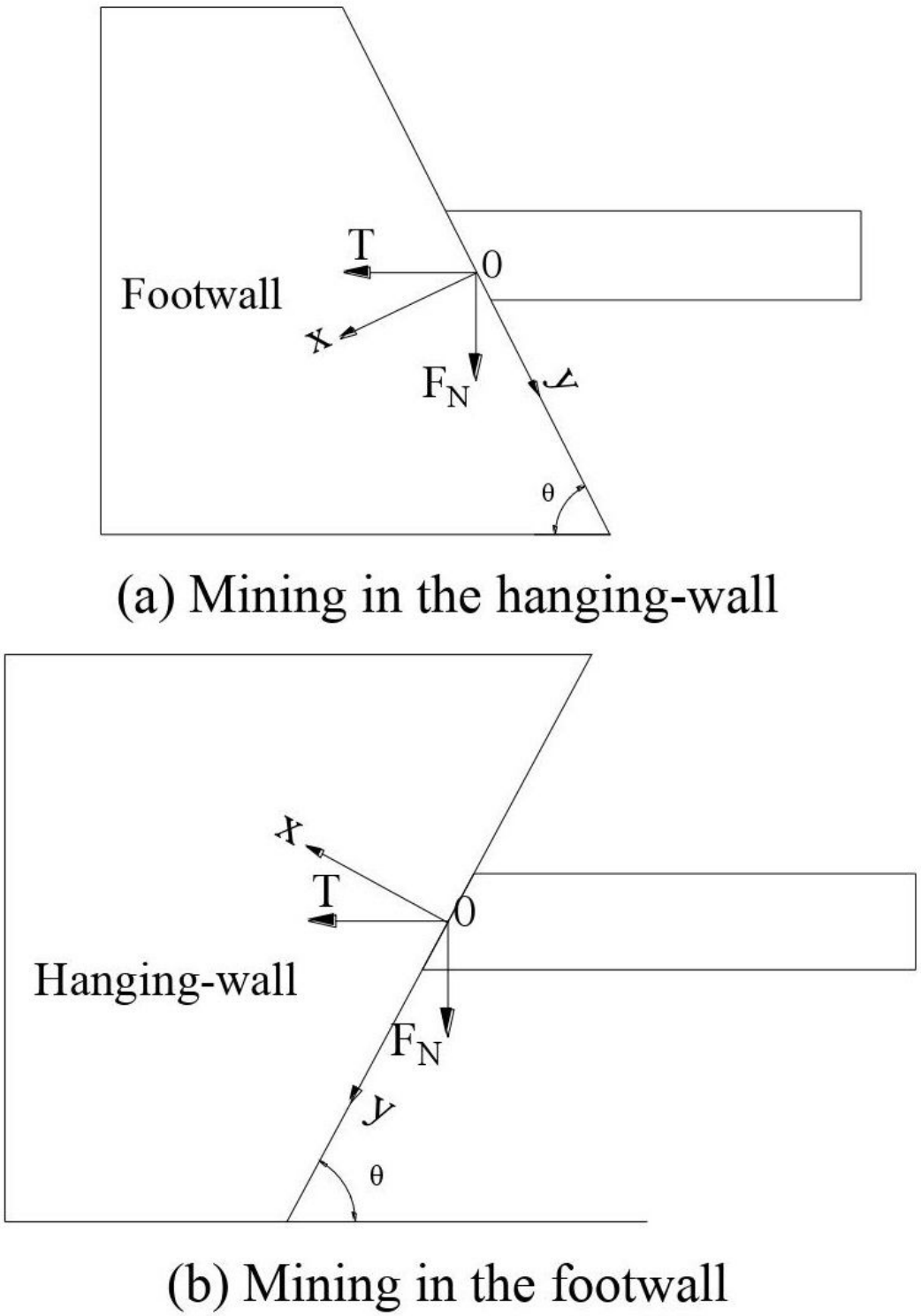

Figure 1

Free-body diagram during mining in the hanging-wall and footwall

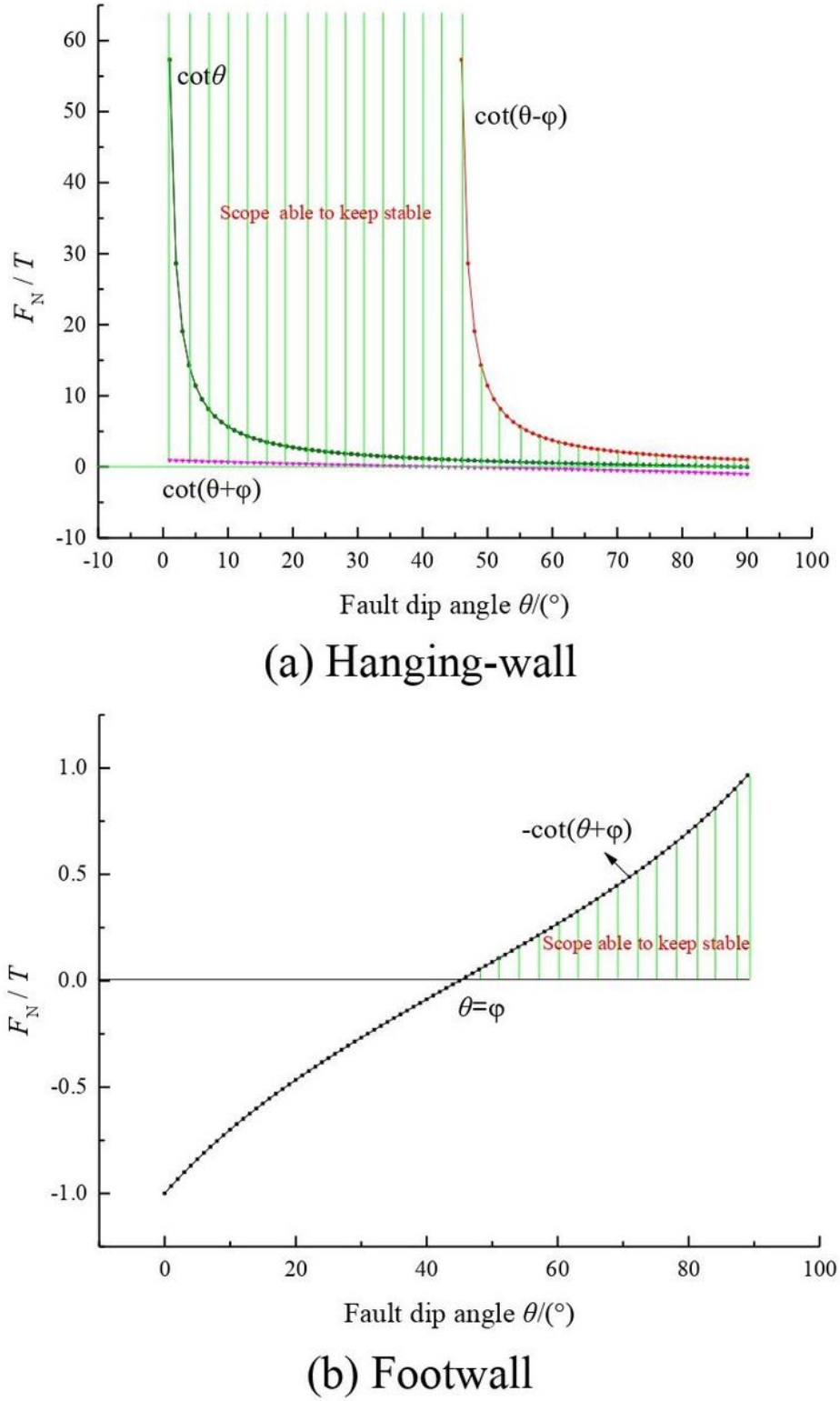

Figure 2

Stable ranges during mining in the hanging-wall and footwall at different fault dip angles θ

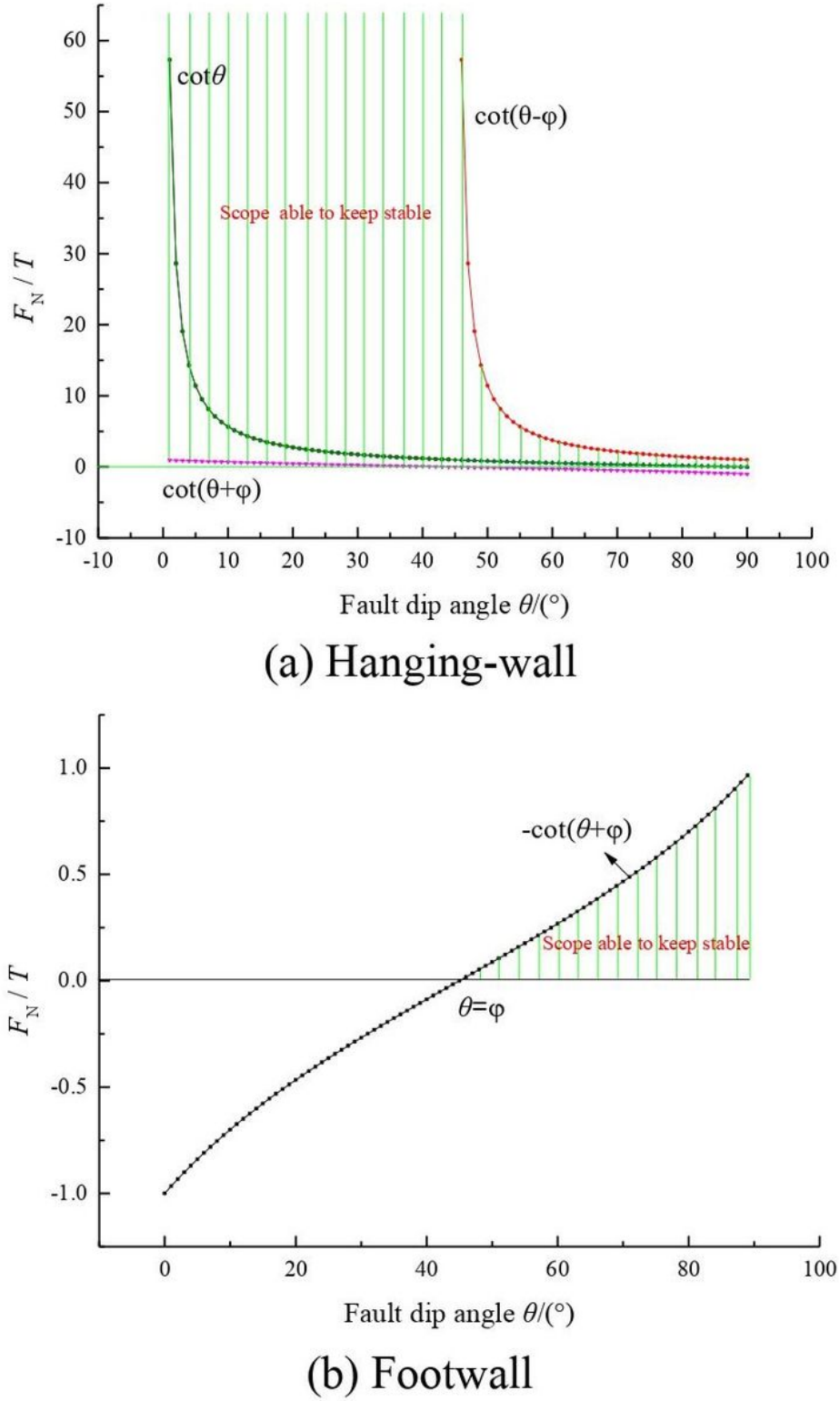

Figure 2

Stable ranges during mining in the hanging-wall and footwall at different fault dip angles θ

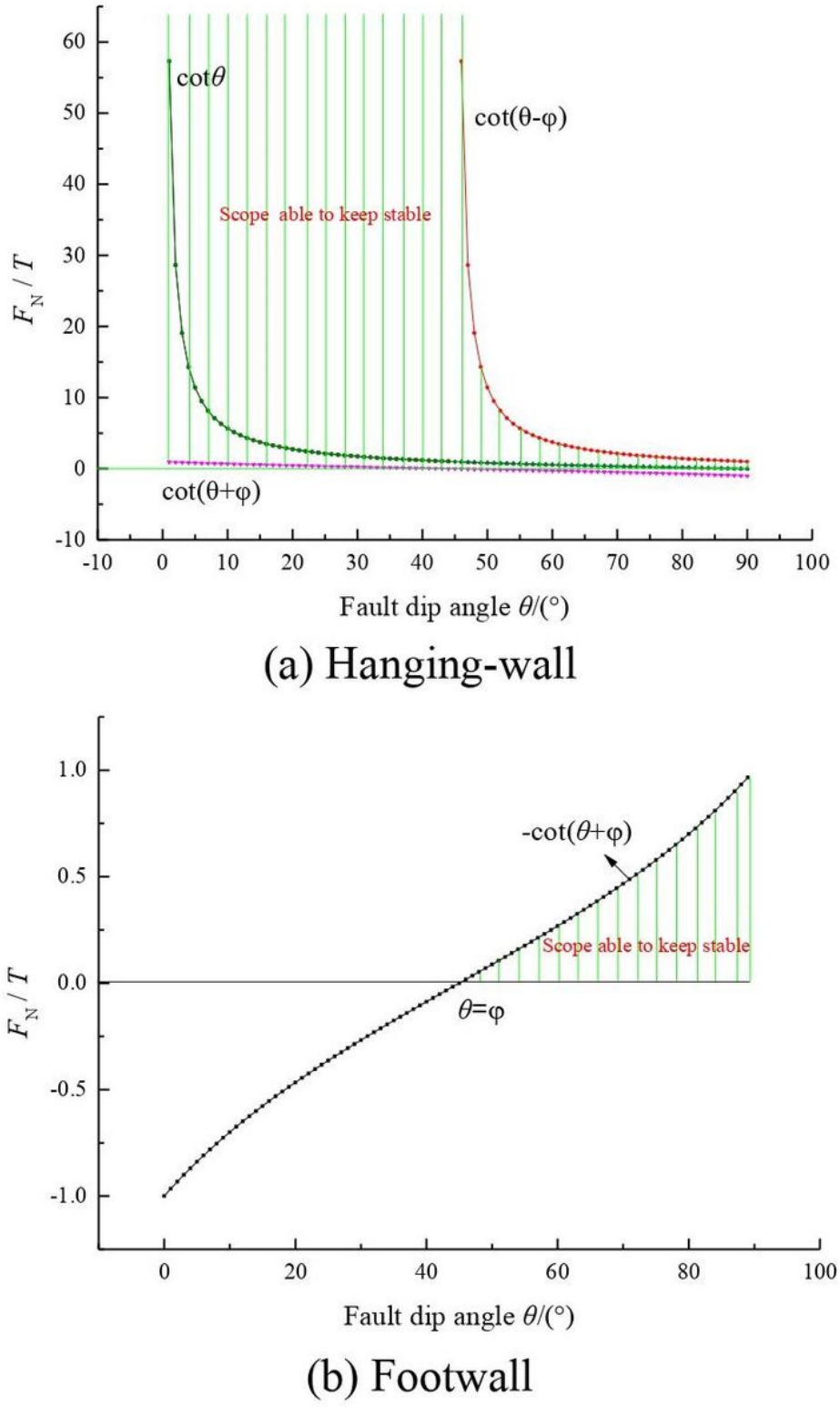

Figure 2

Stable ranges during mining in the hanging-wall and footwall at different fault dip angles θ

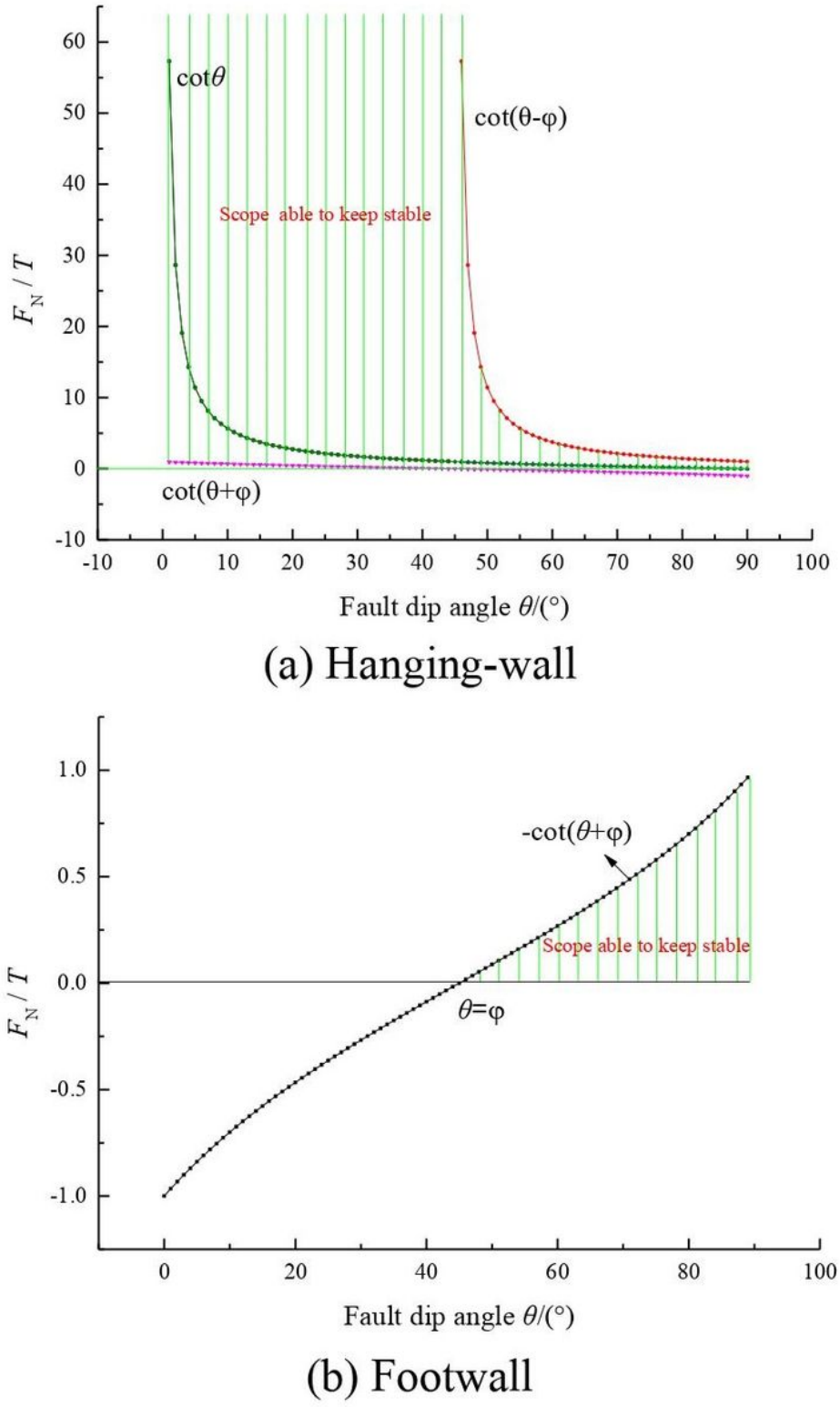

Figure 2

Stable ranges during mining in the hanging-wall and footwall at different fault dip angles θ

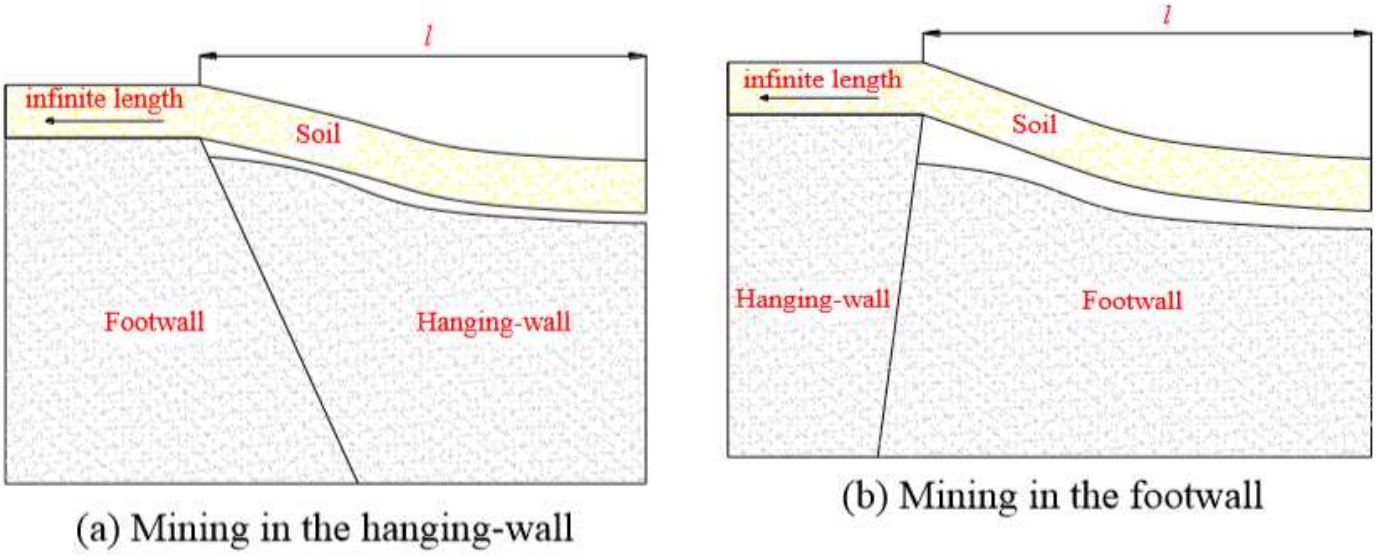

Figure 3

Cantilever beam formed by the soil mass during mining in the hanging-wall and footwall

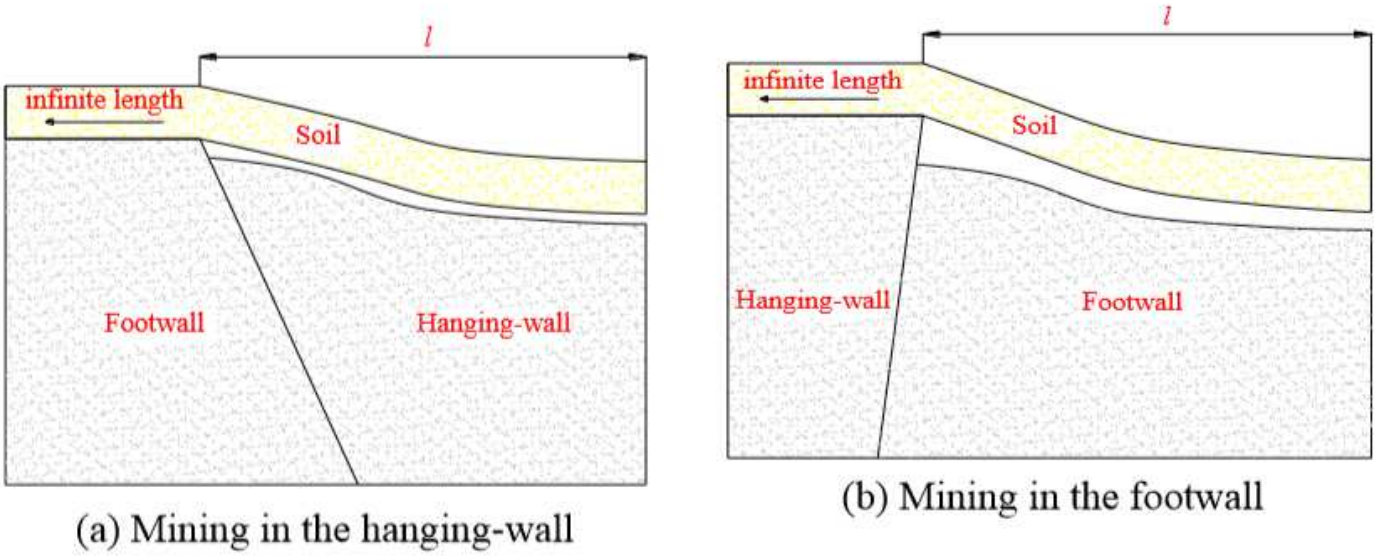

Figure 3

Cantilever beam formed by the soil mass during mining in the hanging-wall and footwall

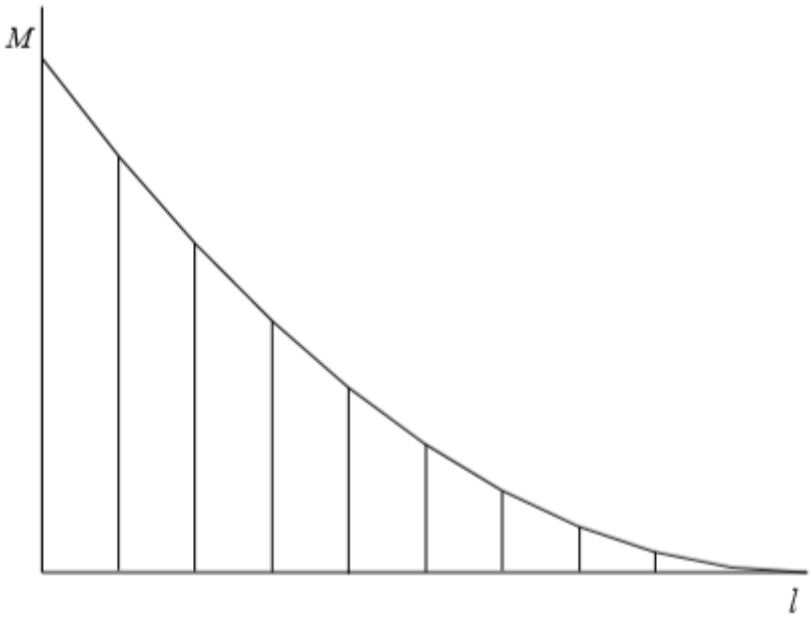

Figure 4

Bending moment on the soil mass in the cantilever

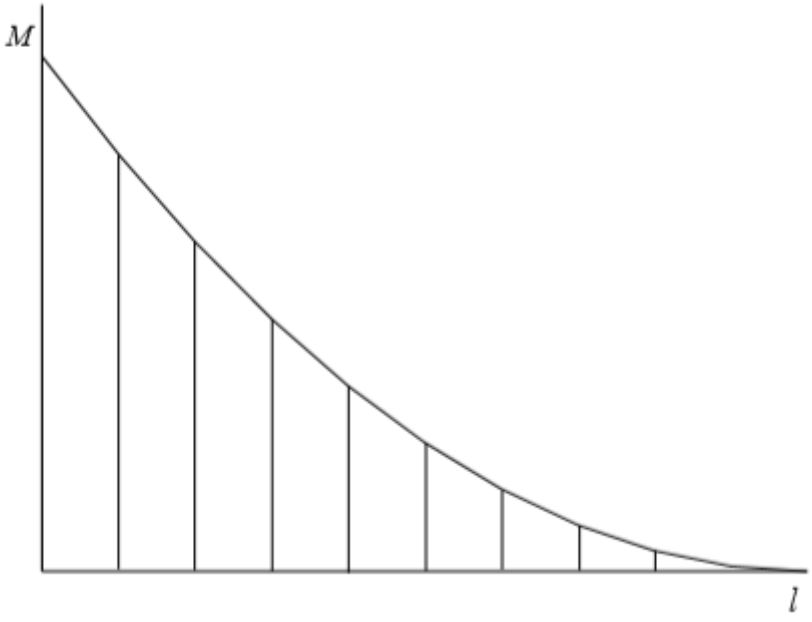

Figure 4

Bending moment on the soil mass in the cantilever

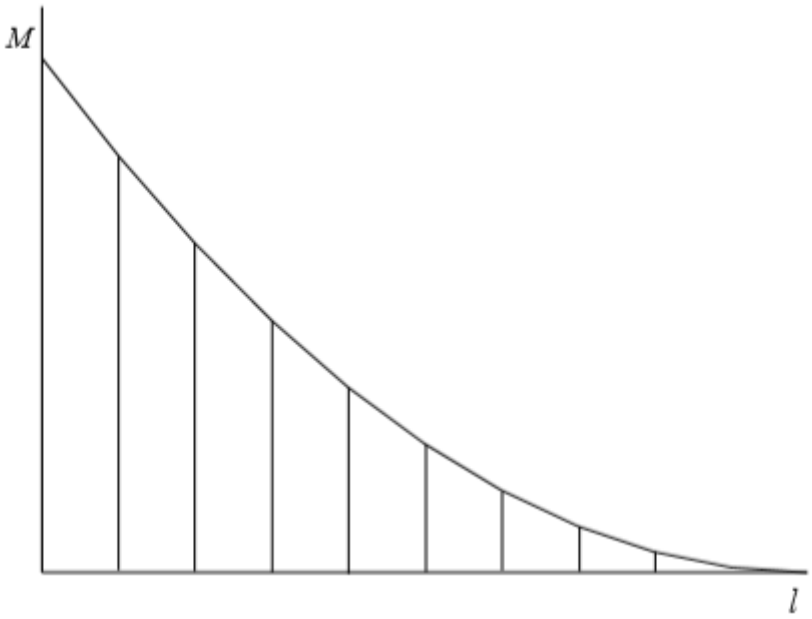

Figure 4

Bending moment on the soil mass in the cantilever

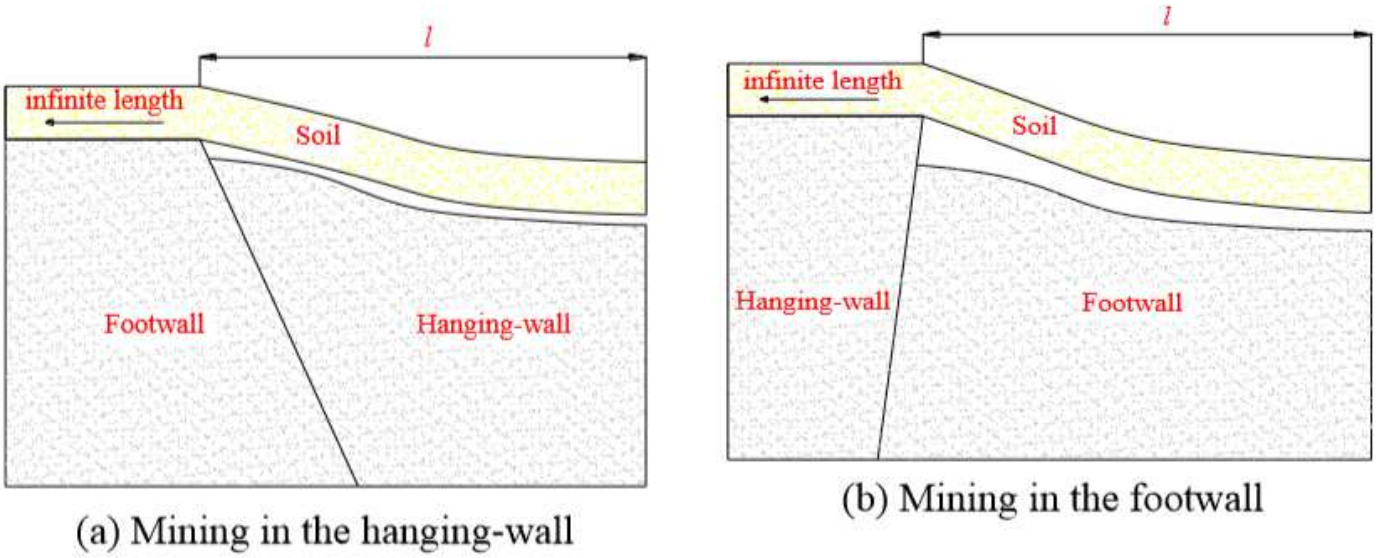

Figure 5

Cantilever beam formed by the soil mass during mining in the hanging-wall and footwall

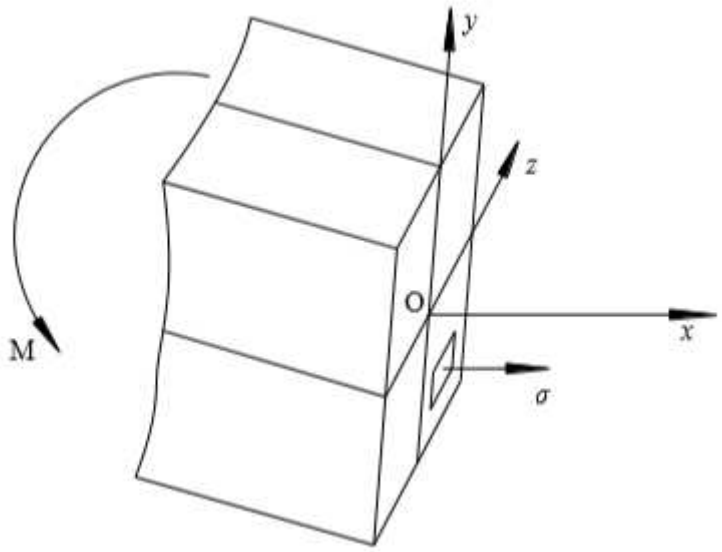

Figure 5

Internal stress of soil mass cantilever section

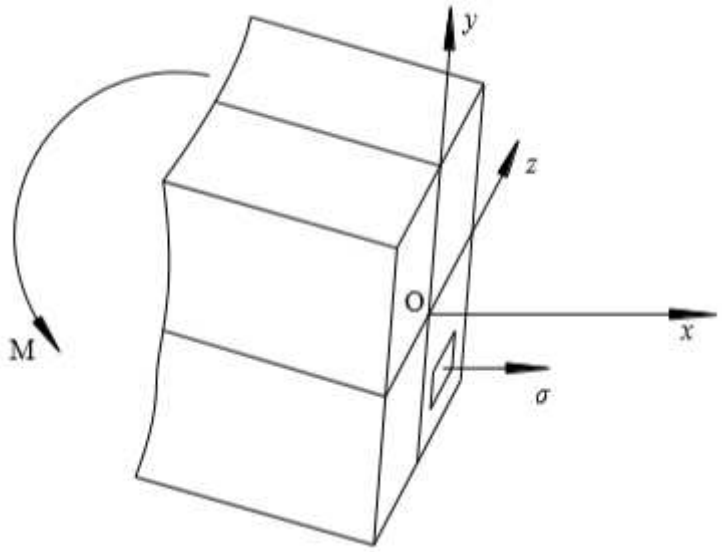

Figure 5

Internal stress of soil mass cantilever section

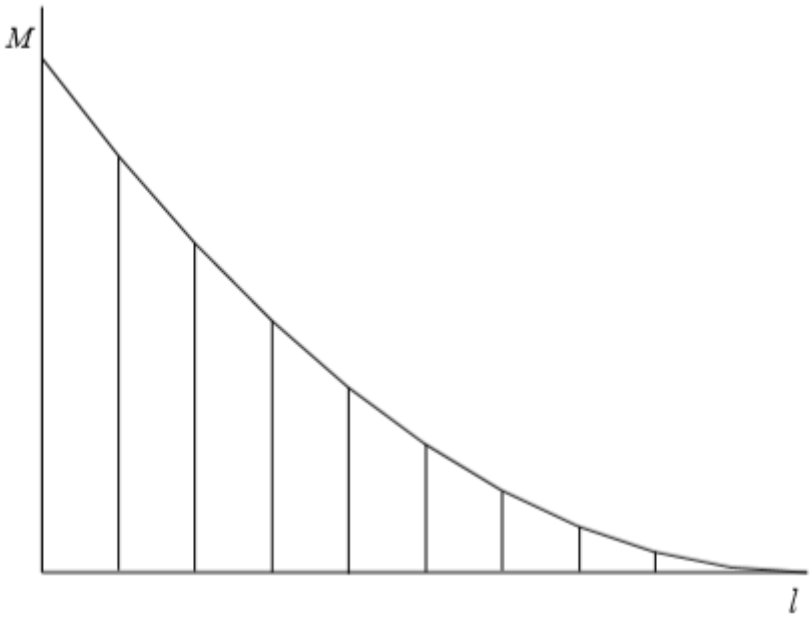

Figure 6

Bending moment on the soil mass in the cantilever

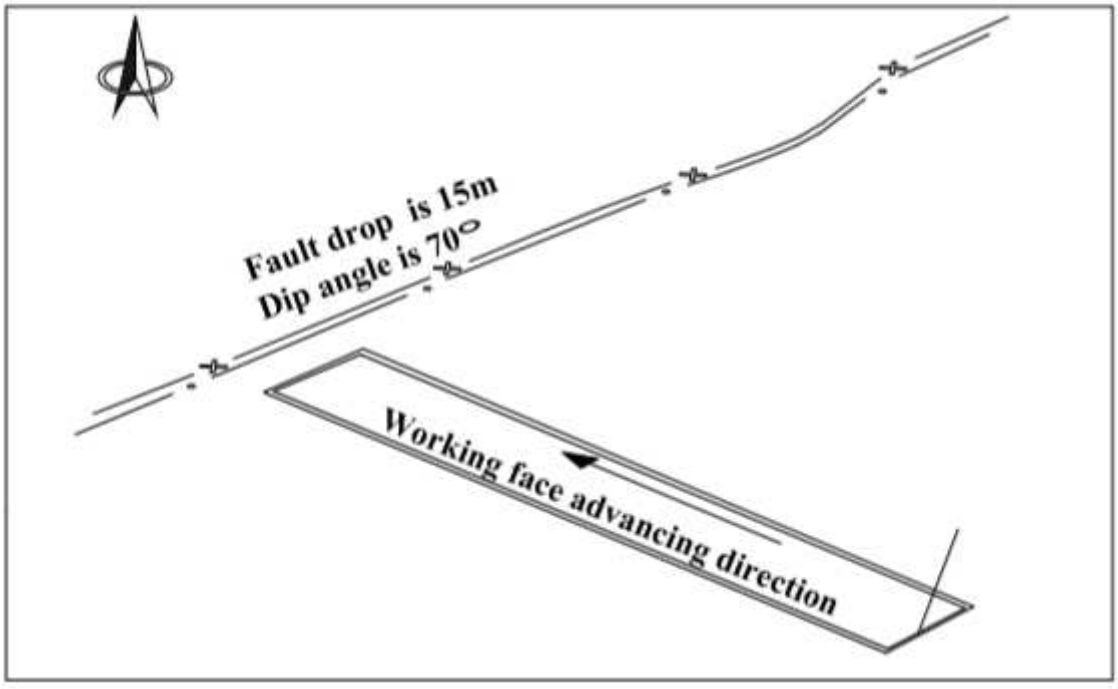

Figure 6

Relative position of fault and working face

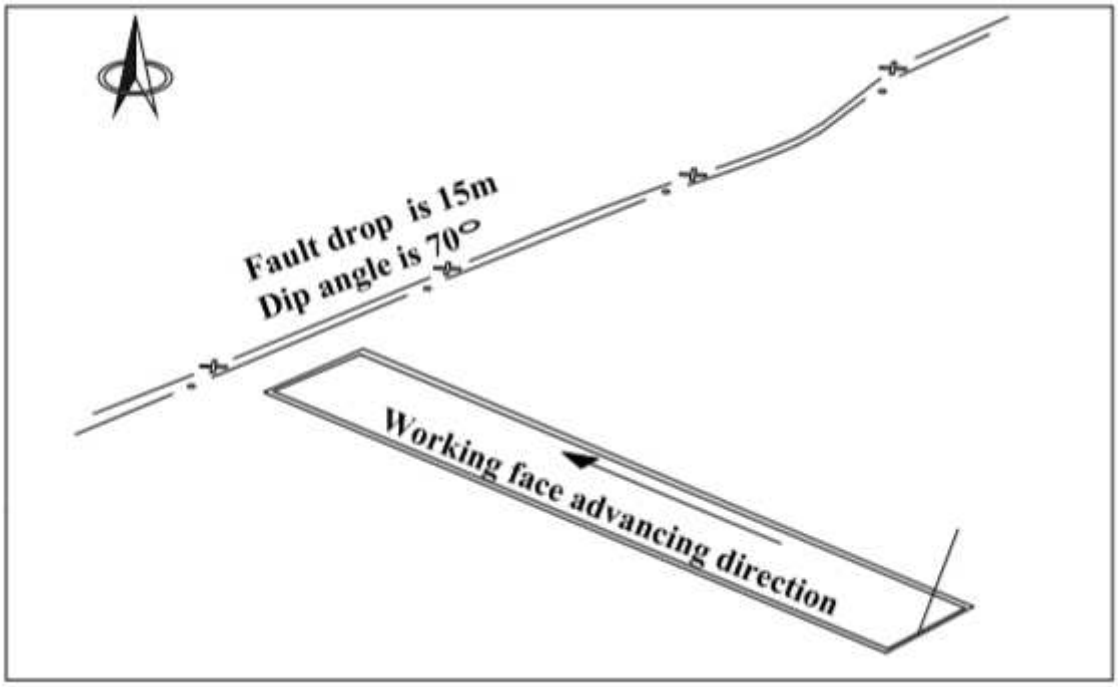

Figure 6

Relative position of fault and working face

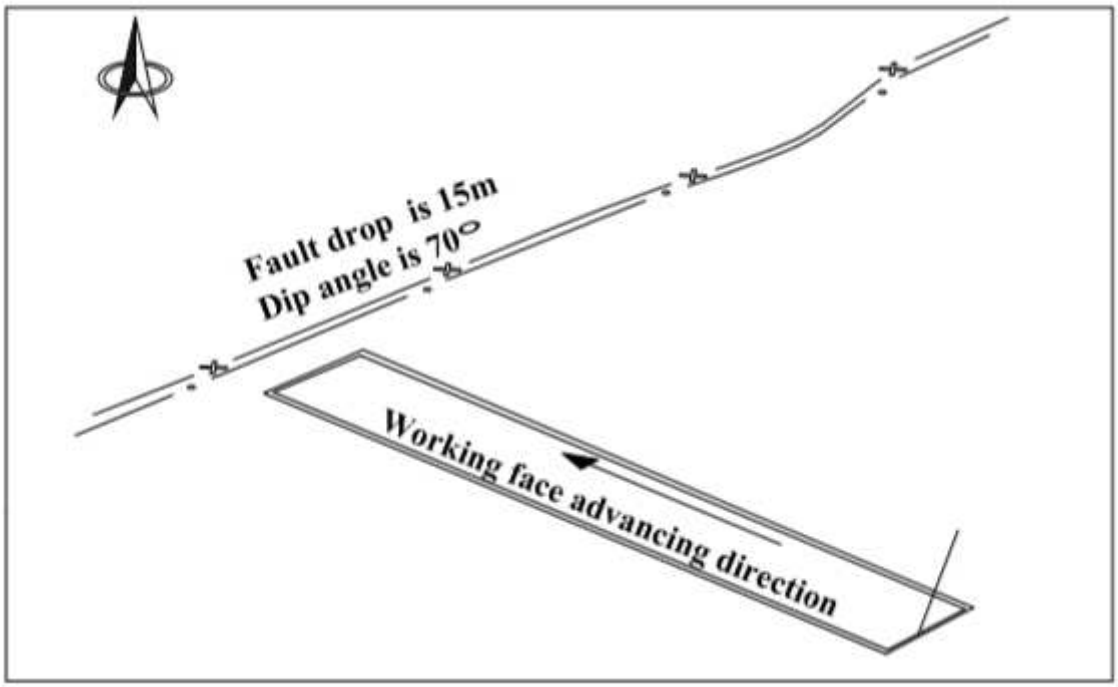

Figure 6

Relative position of fault and working face

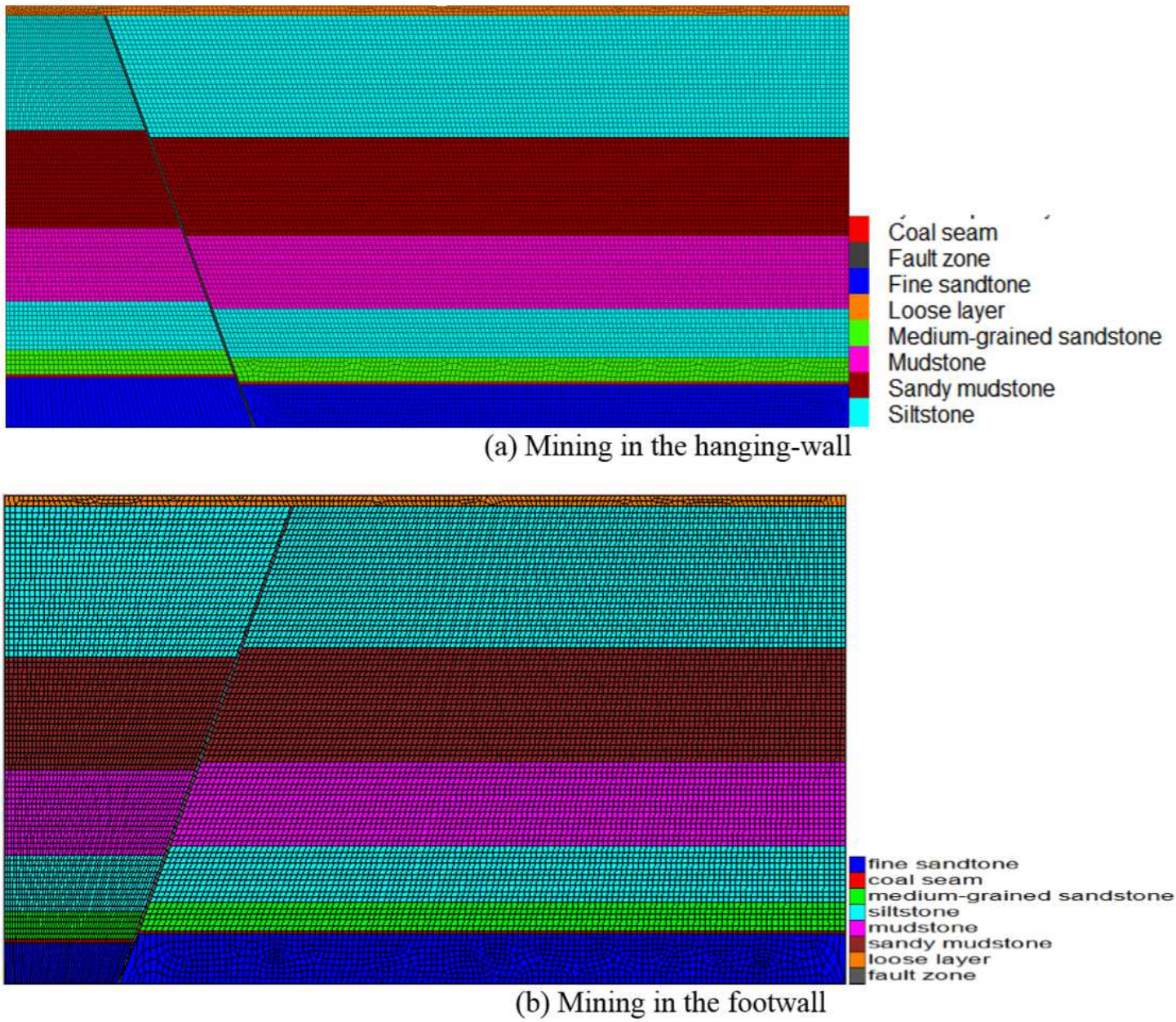

Figure 7

Simulation models when mining in the hanging-wall and footwall

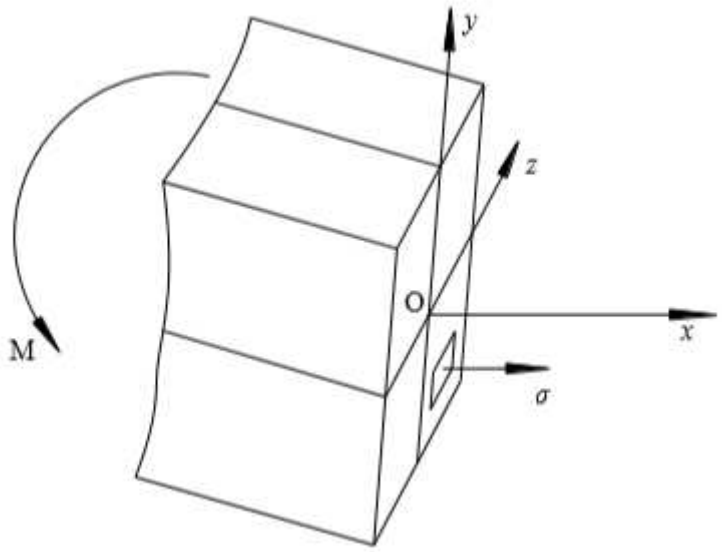

Figure 7

Internal stress of soil mass cantilever section

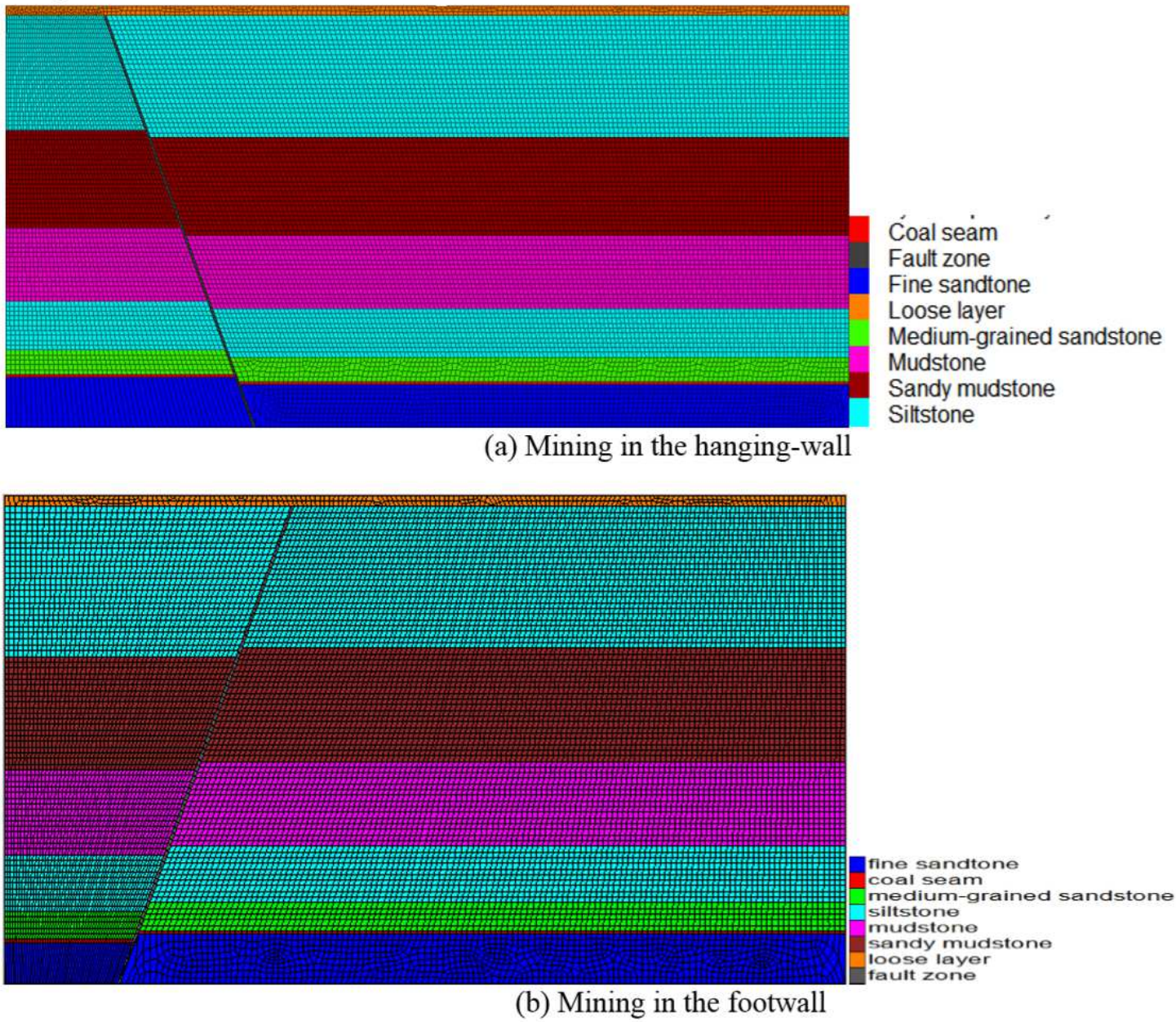

Figure 7

Simulation models when mining in the hanging-wall and footwall

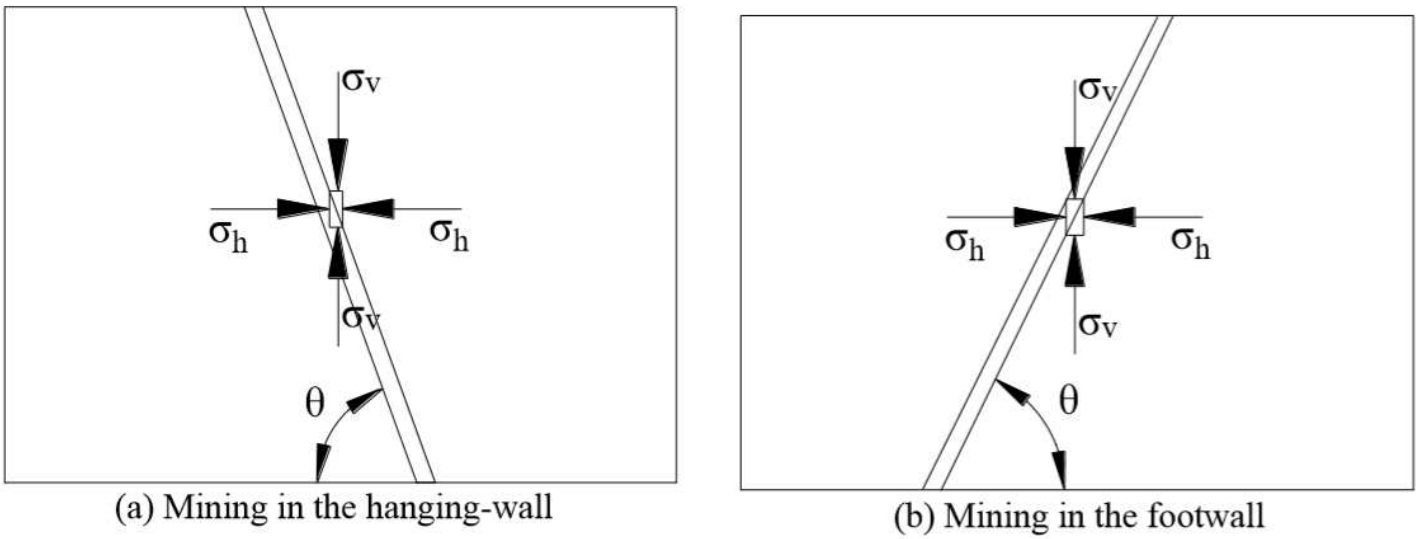

Figure 8

Diagram of the normal and shear stress calculation when mining in the hangingwall and footwall

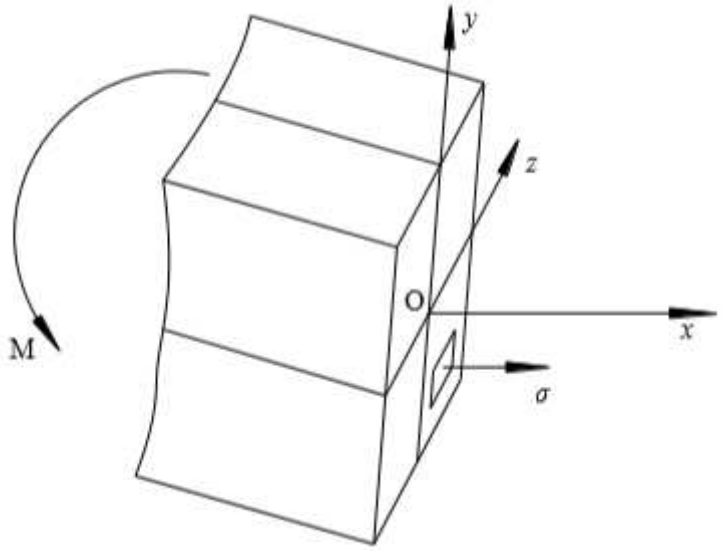

Figure 8

Internal stress of soil mass cantilever section

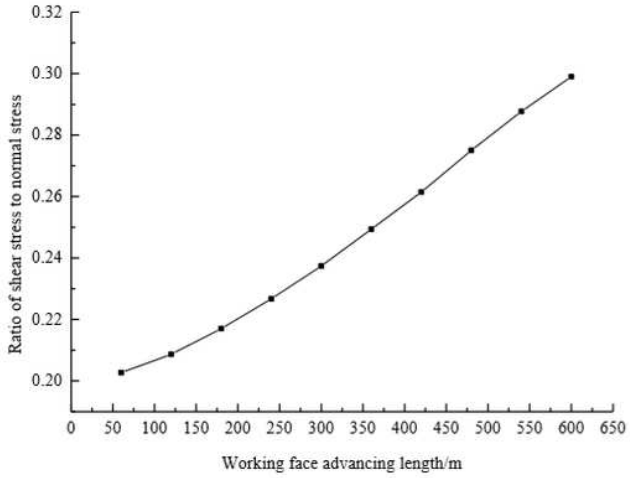

(a) Mining in the hanging-wall

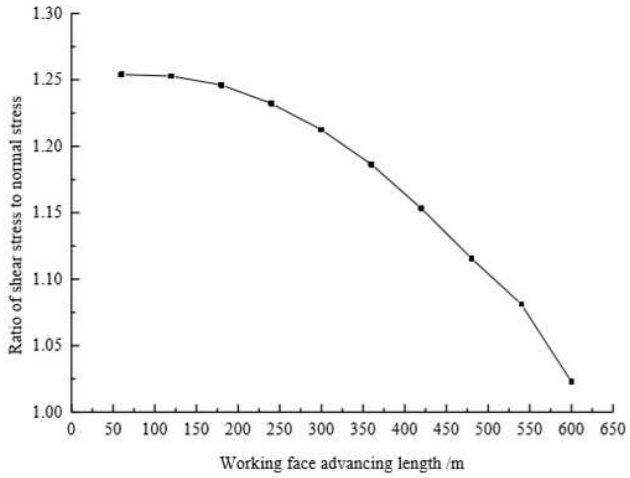

(b) Mining in the footwall

Figure 9

Ratios of shear stress to normal stress on the rock mass in the fault zone at the fault outcrop in the progress of advancing to the working face to a fault

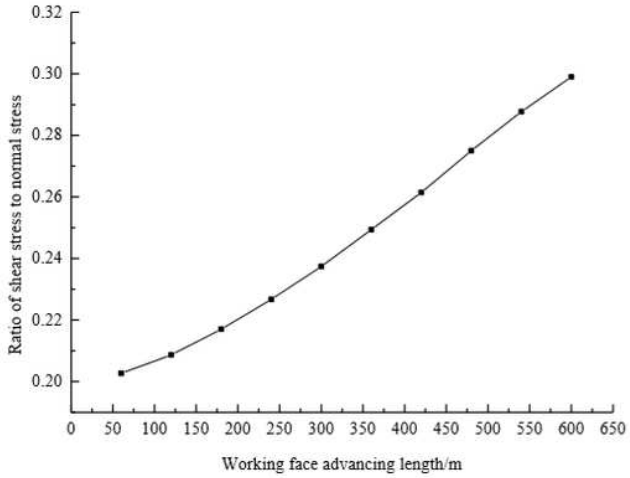

(a) Mining in the hanging-wall

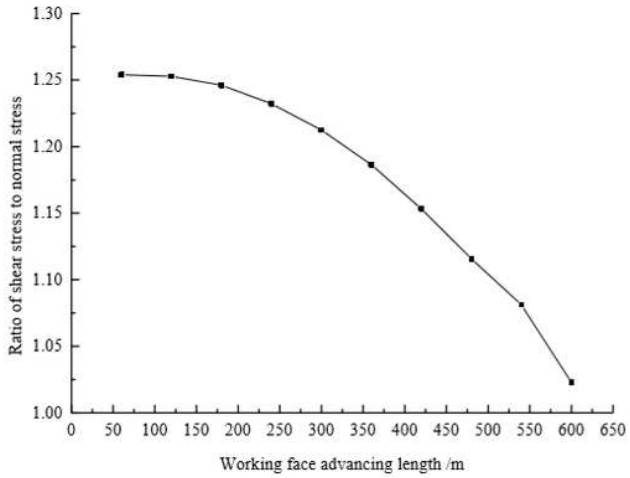

(b) Mining in the footwall

Figure 9

Ratios of shear stress to normal stress on the rock mass in the fault zone at the fault outcrop in the progress of advancing to the working face to a fault

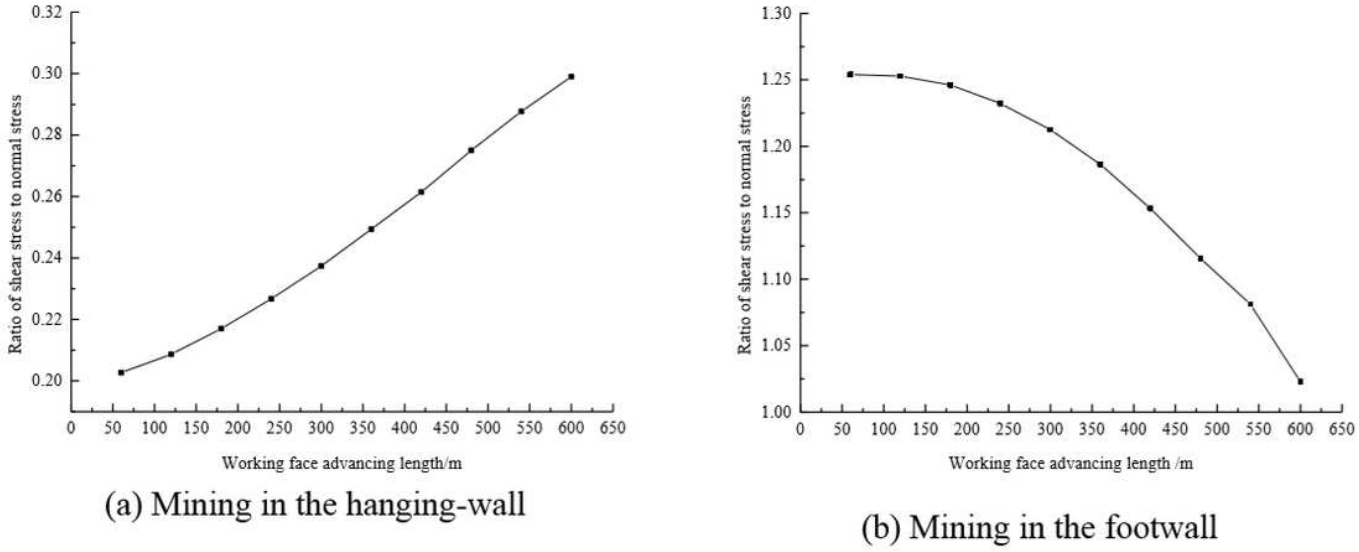

Figure 9

Ratios of shear stress to normal stress on the rock mass in the fault zone at the fault outcrop in the progress of advancing to the working face to a fault

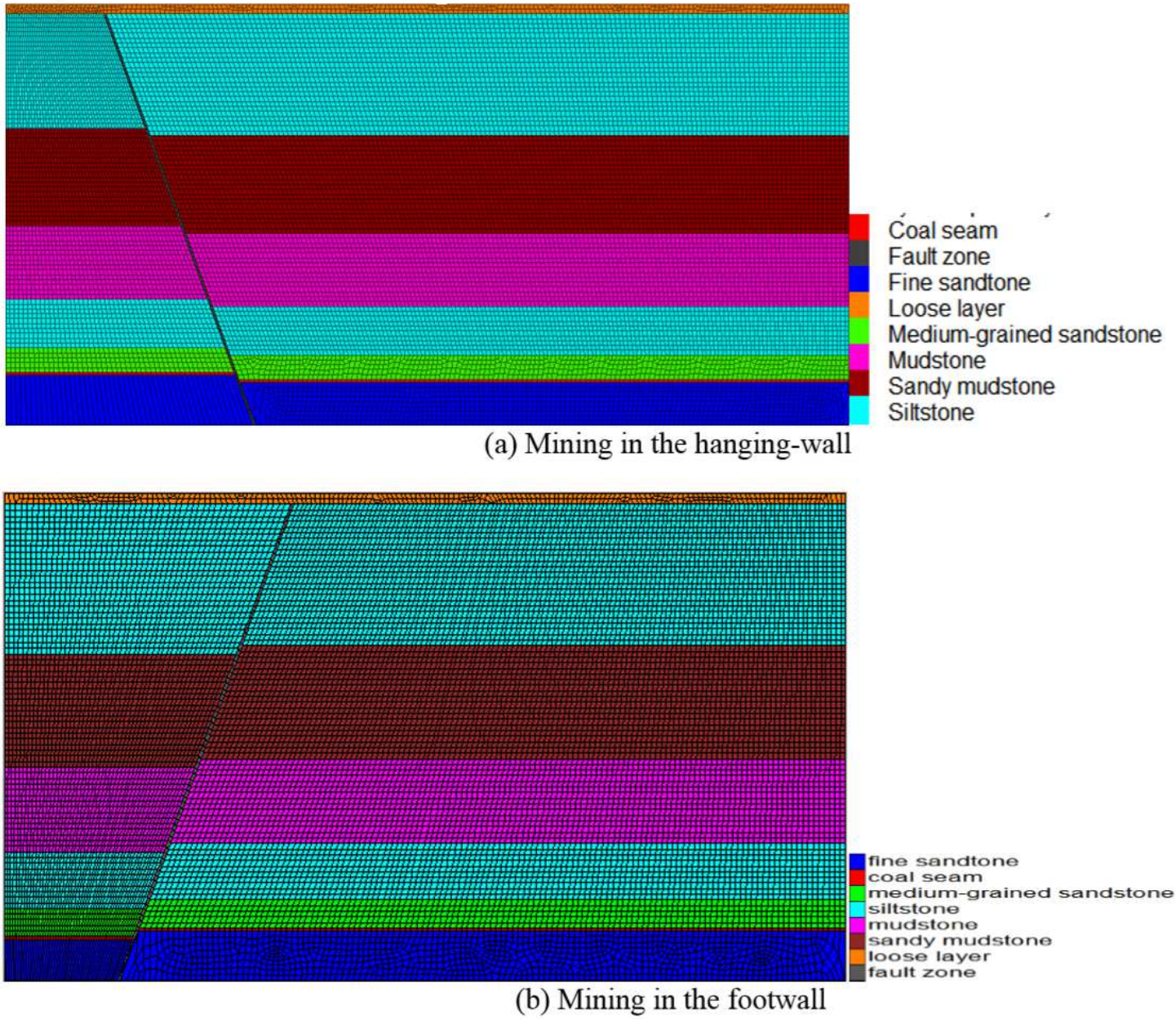

Figure 9

Simulation models when mining in the hanging-wall and footwall

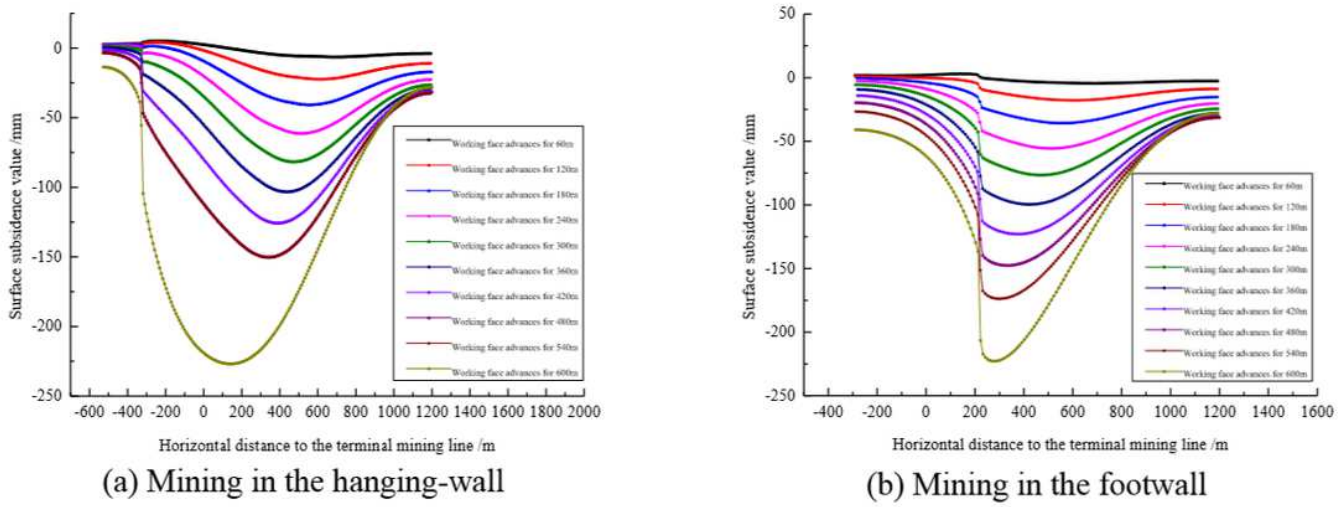

Figure 10

Surface subsidence when advancing the working face to a fault

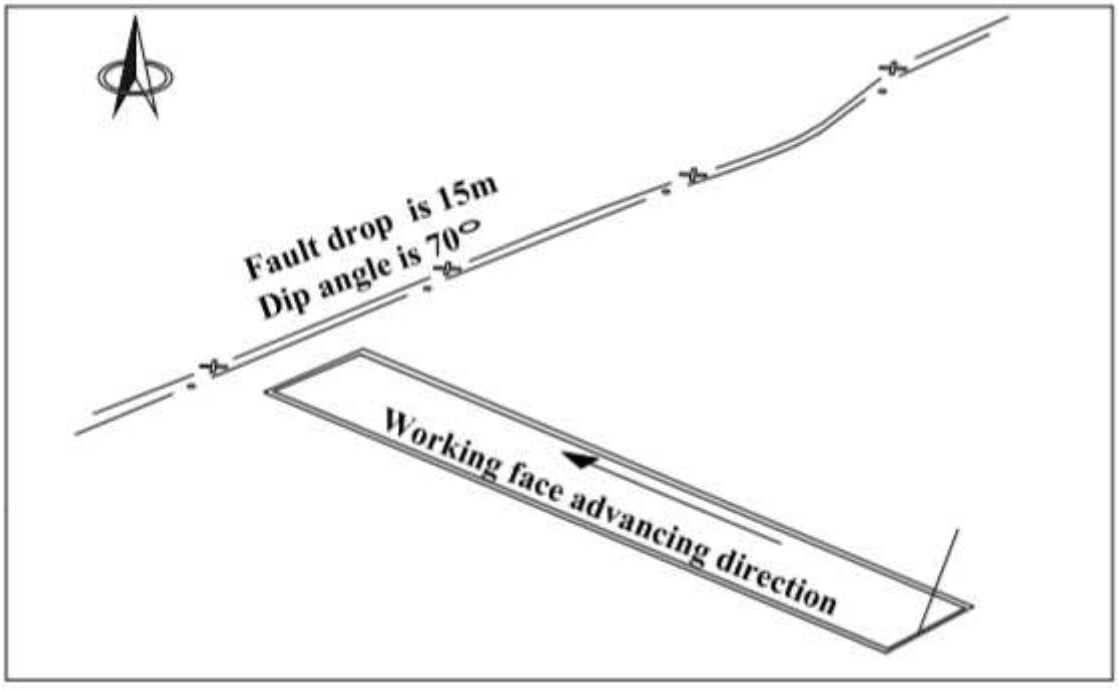

Figure 10

Relative position of fault and working face

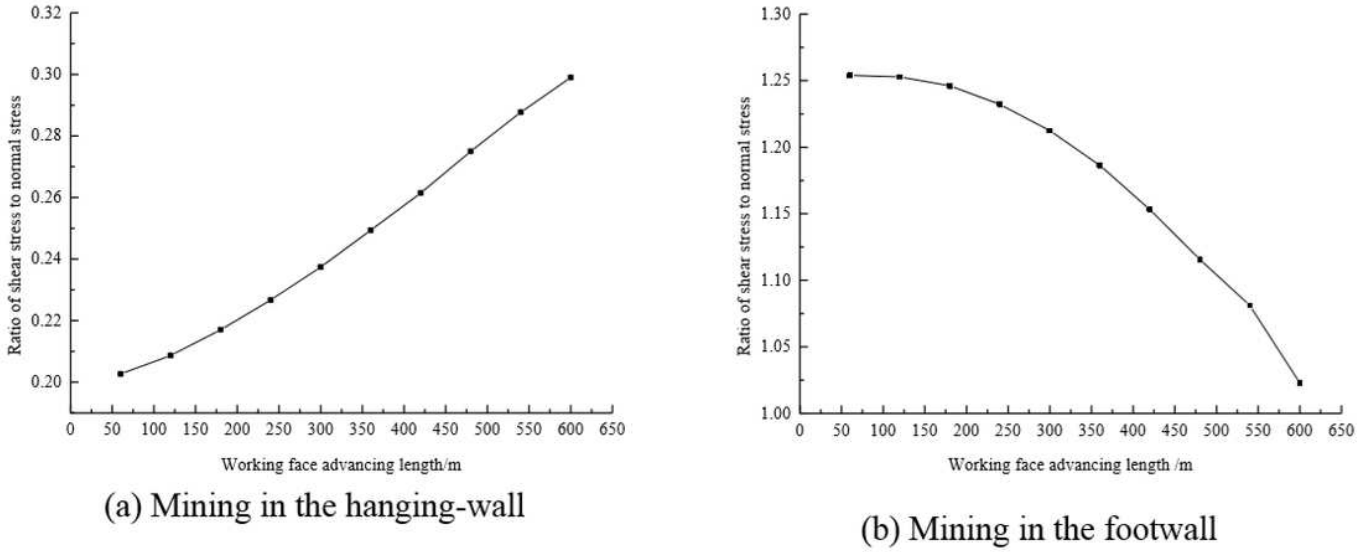

Figure 10

Ratios of shear stress to normal stress on the rock mass in the fault zone at the fault outcrop in the progress of advancing to the working face to a fault

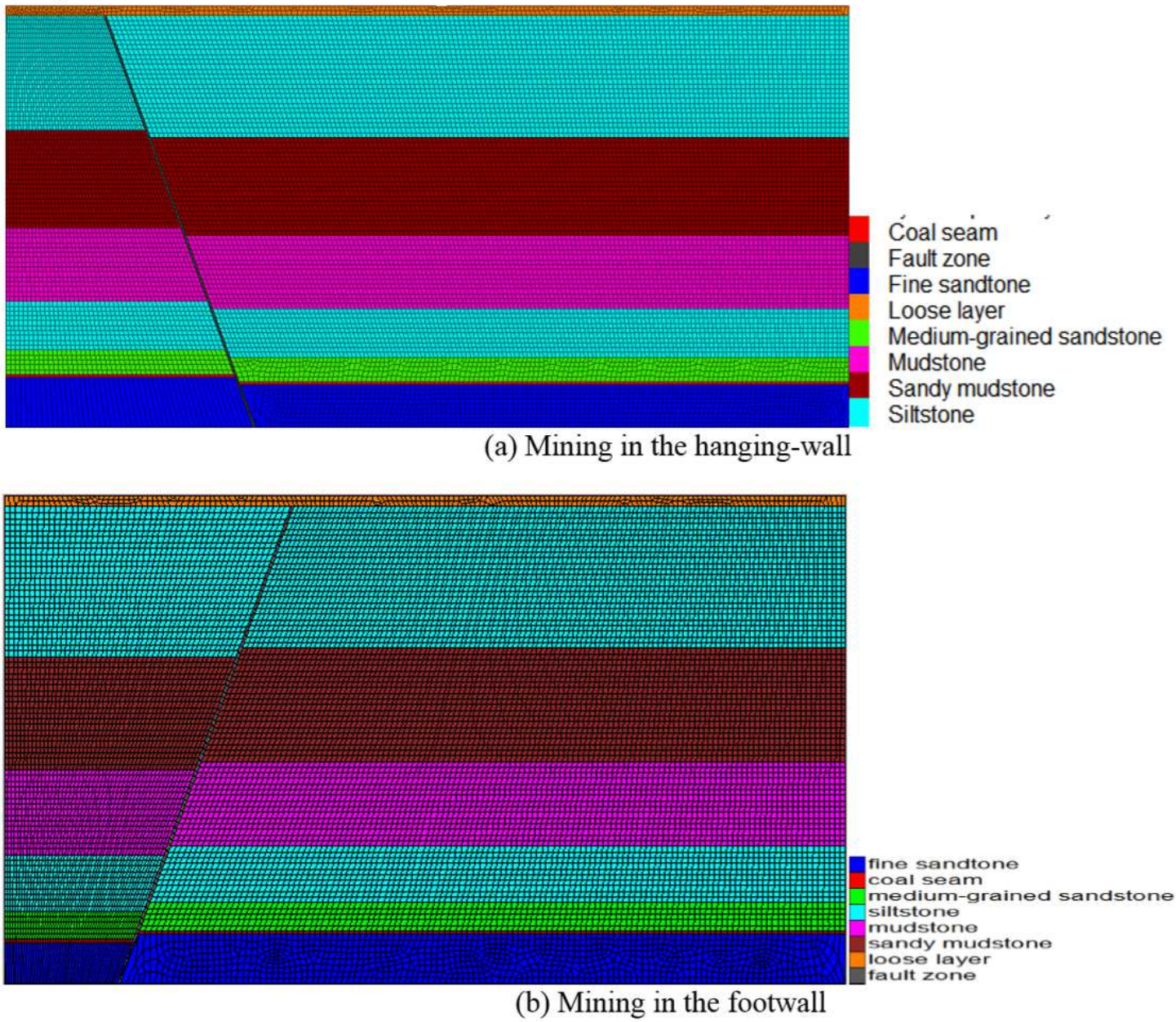

Figure 11

Simulation models when mining in the hanging-wall and footwall

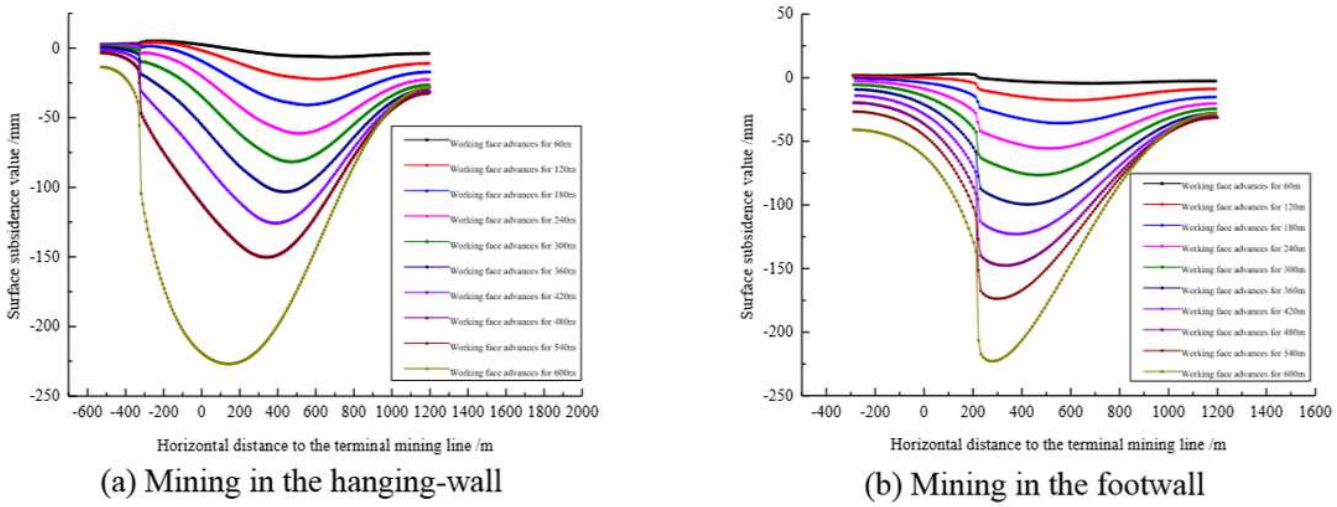

Figure 11

Surface subsidence when advancing the working face to a fault

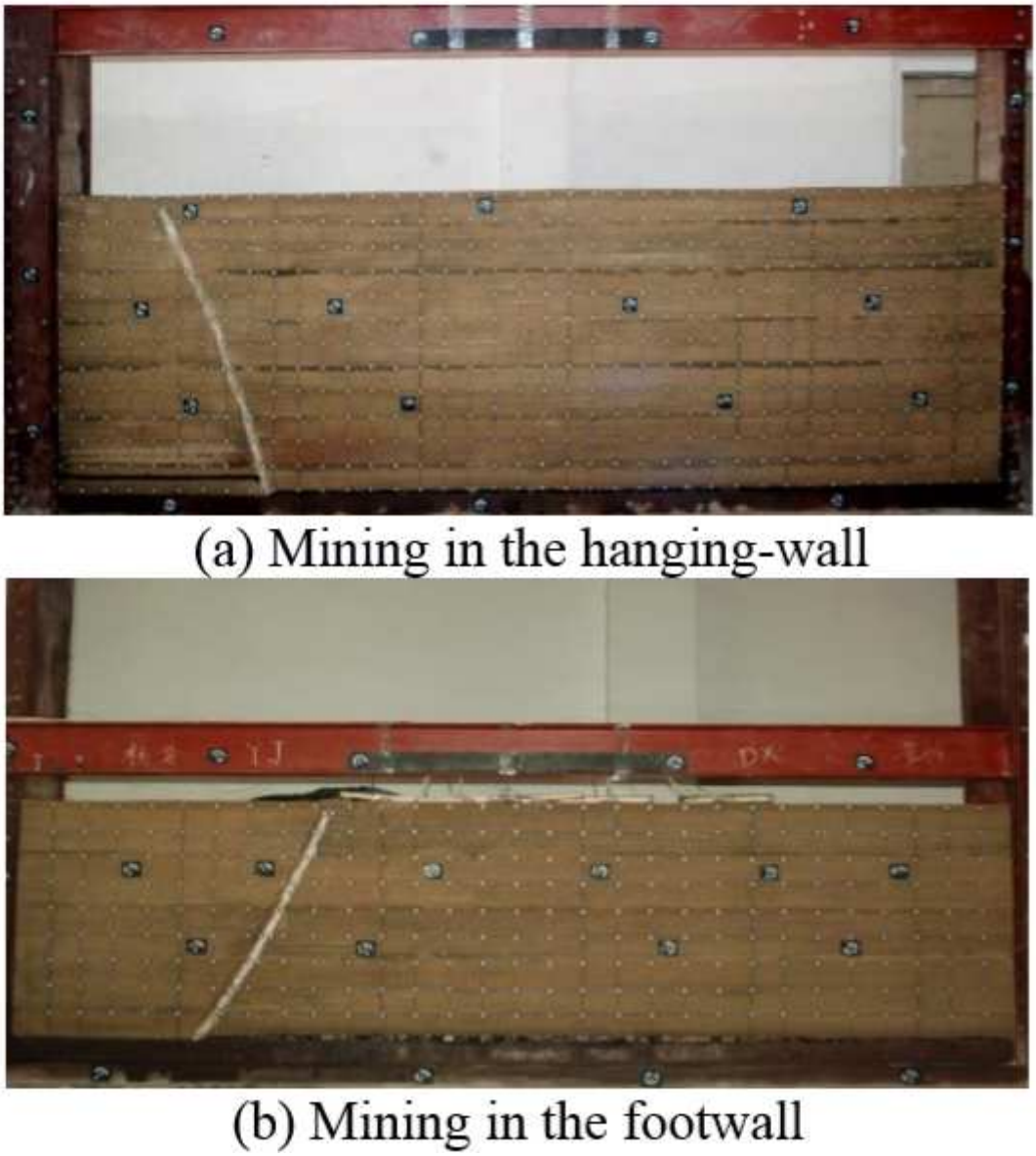

Figure 11

Similarity models when mining in the hanging wall and footwall

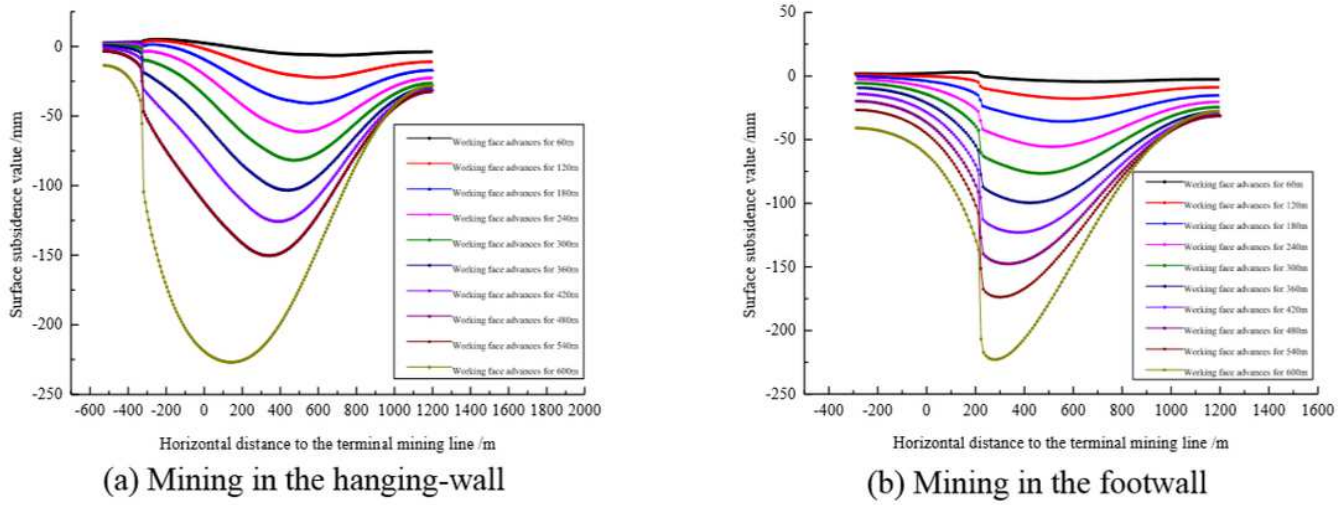

(a) Mining in the hanging-wall

(b) Mining in the footwall

Figure 11

Surface subsidence when advancing the working face to a fault

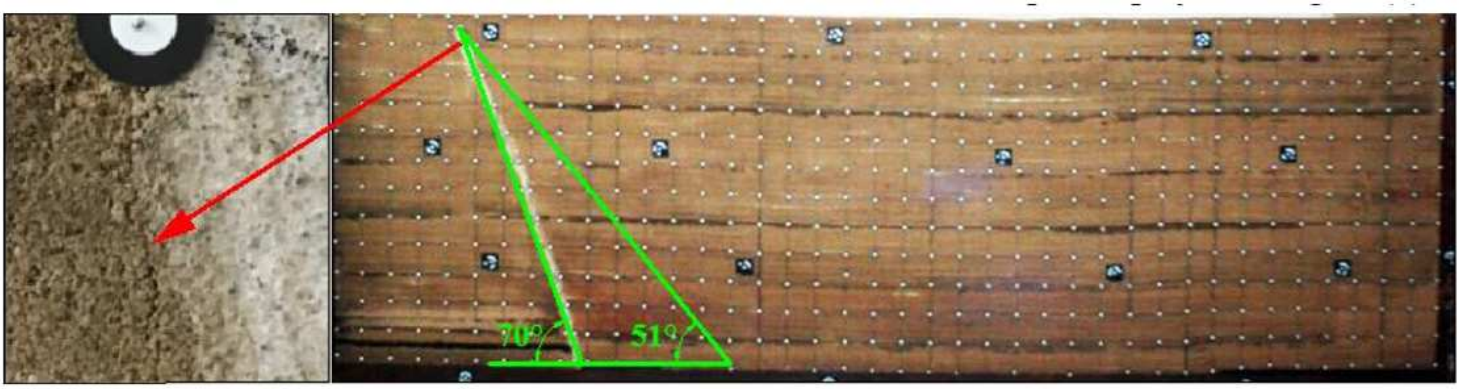

(a) Mining in the hanging-wall

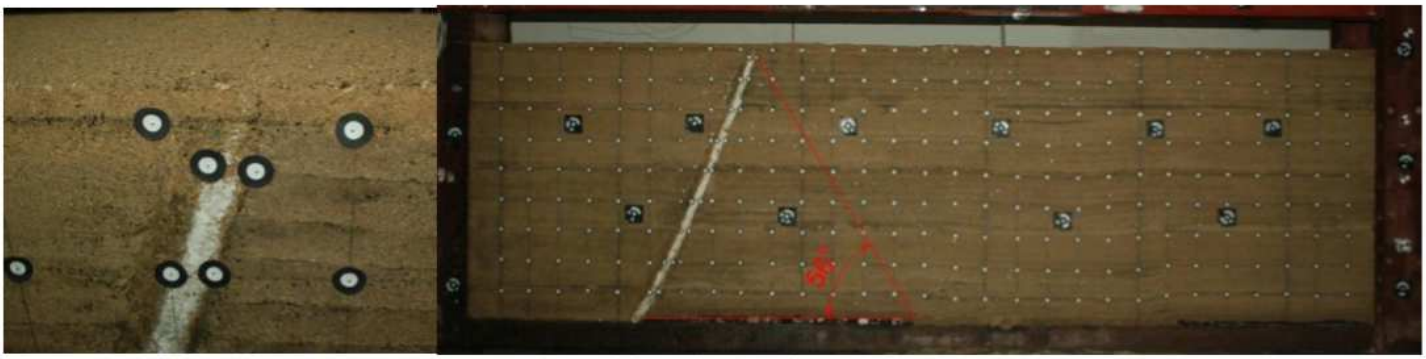

(b) Mining in the footwall

Figure 12

Relative position of the working face and fault when the fault slips

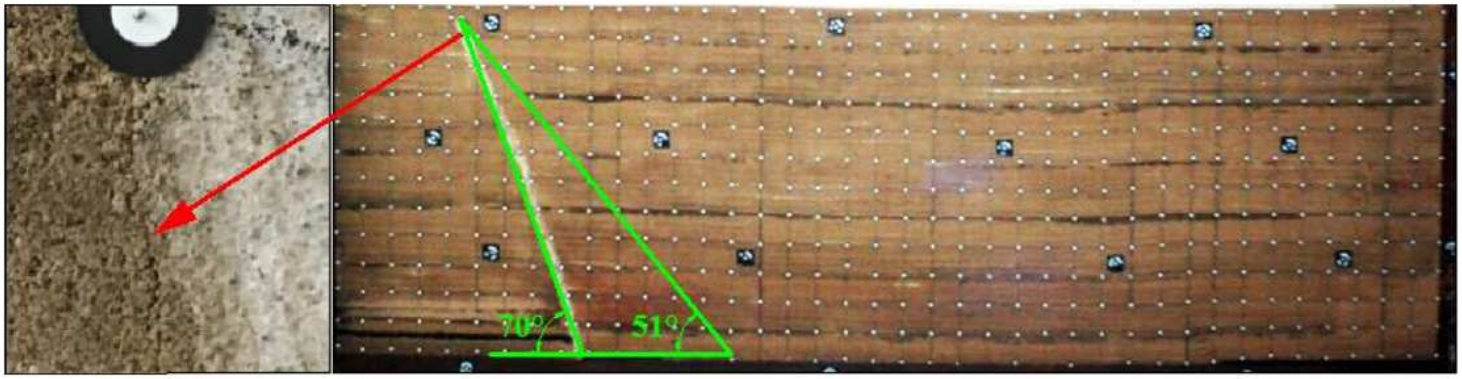

(a) Mining in the hanging-wall

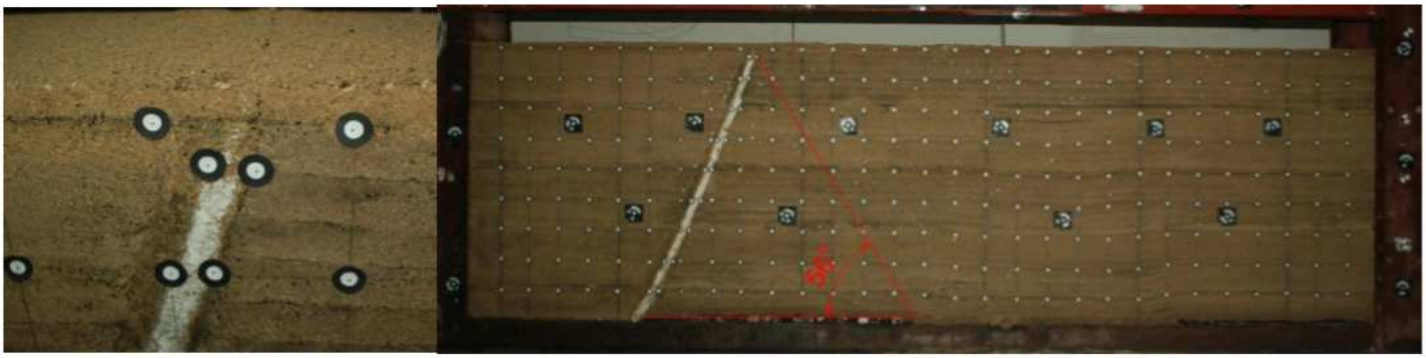

(b) Mining in the footwall

Figure 12

Relative position of the working face and fault when the fault slips

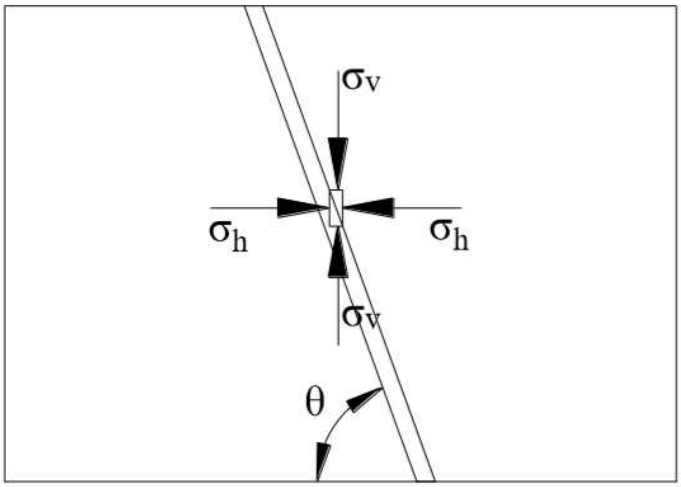

(a) Mining in the hanging-wall

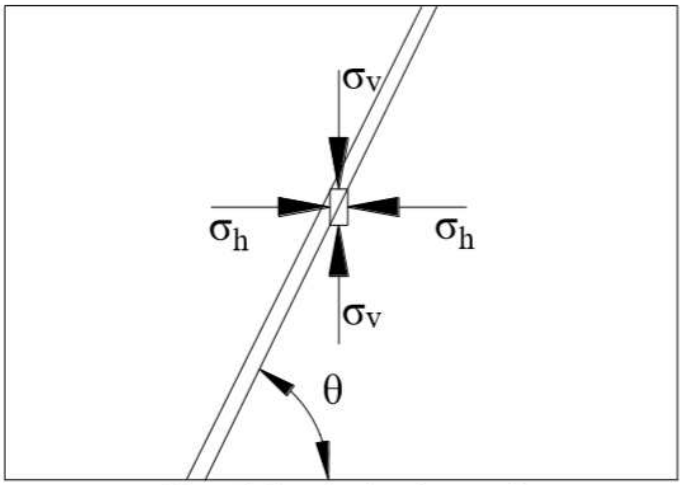

(b) Mining in the footwall

Figure 12

Diagram of the normal and shear stress calculation when mining in the hangingwall and footwall

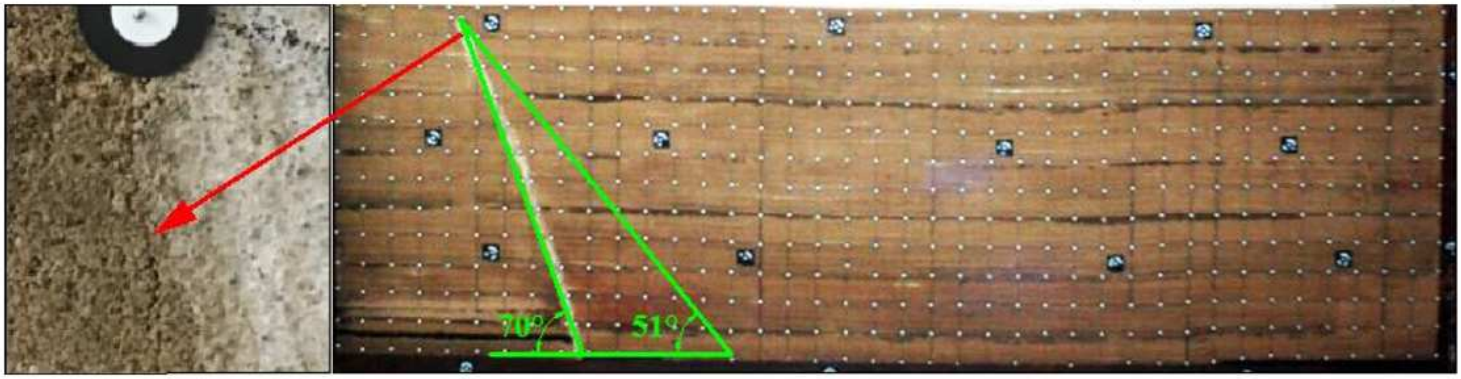

(a) Mining in the hanging-wall

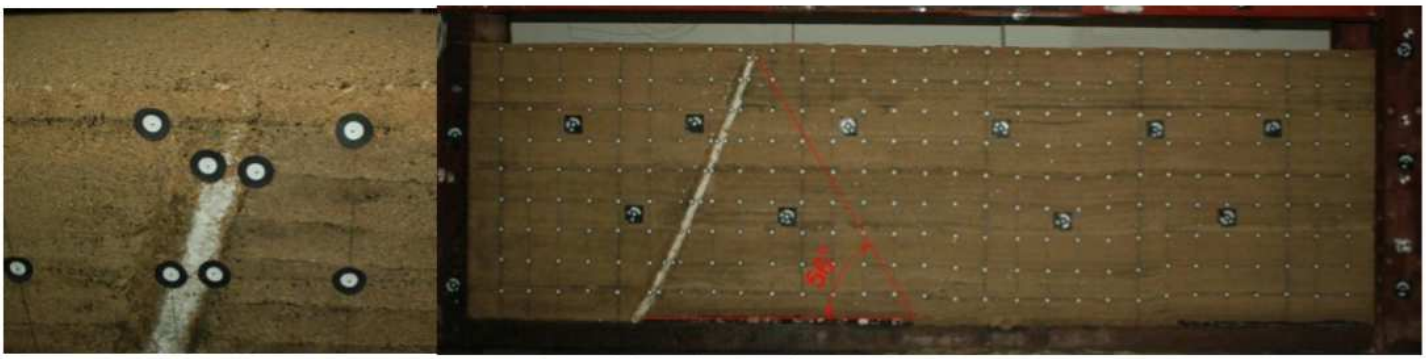

(b) Mining in the footwall

Figure 12

Relative position of the working face and fault when the fault slips

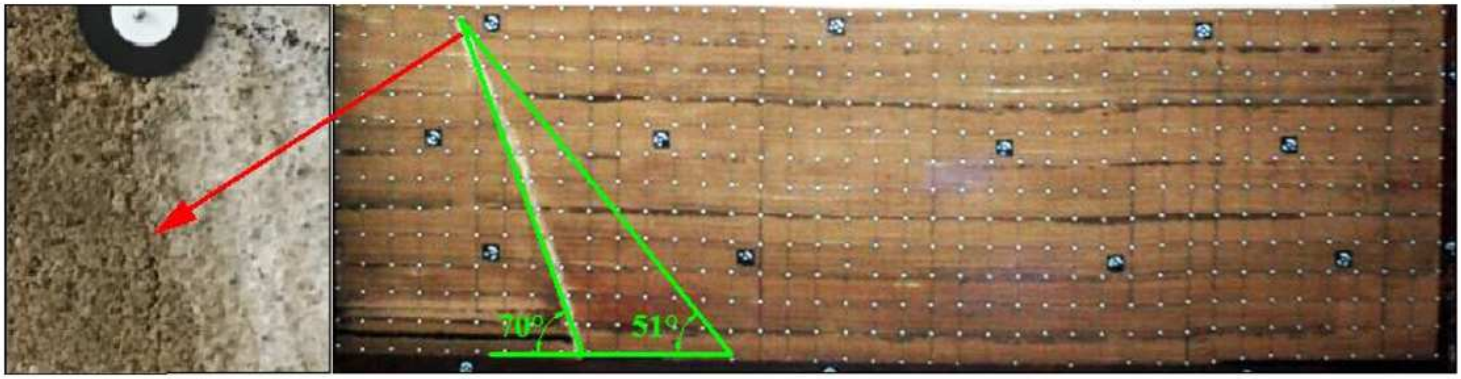

(a) Mining in the hanging-wall

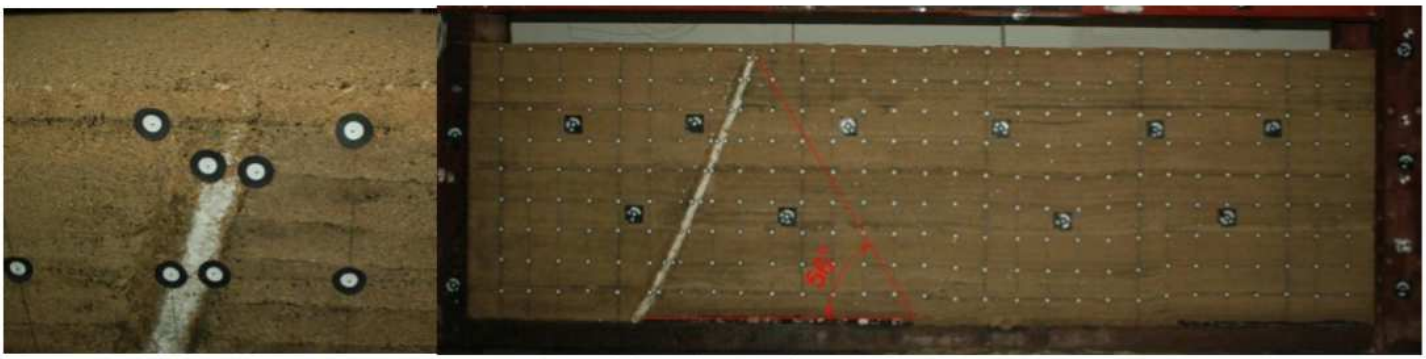

(b) Mining in the footwall

Figure 13

Relative position of the working face and fault when the fault slips

(a) Mining in the hanging-wall

(b) Mining in the footwall

Figure 13

Fractures in the surface at fault outcrop when mining is finished

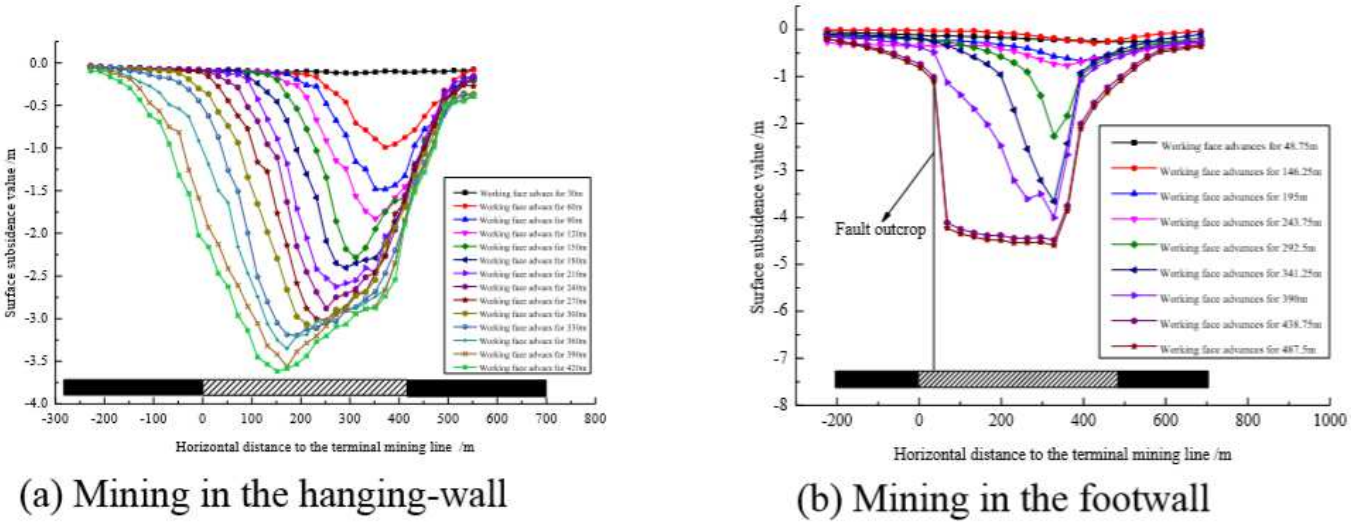

(a) Mining in the hanging-wall

(b) Mining in the footwall

Figure 14

Surface subsidence profiles when advancing the working face

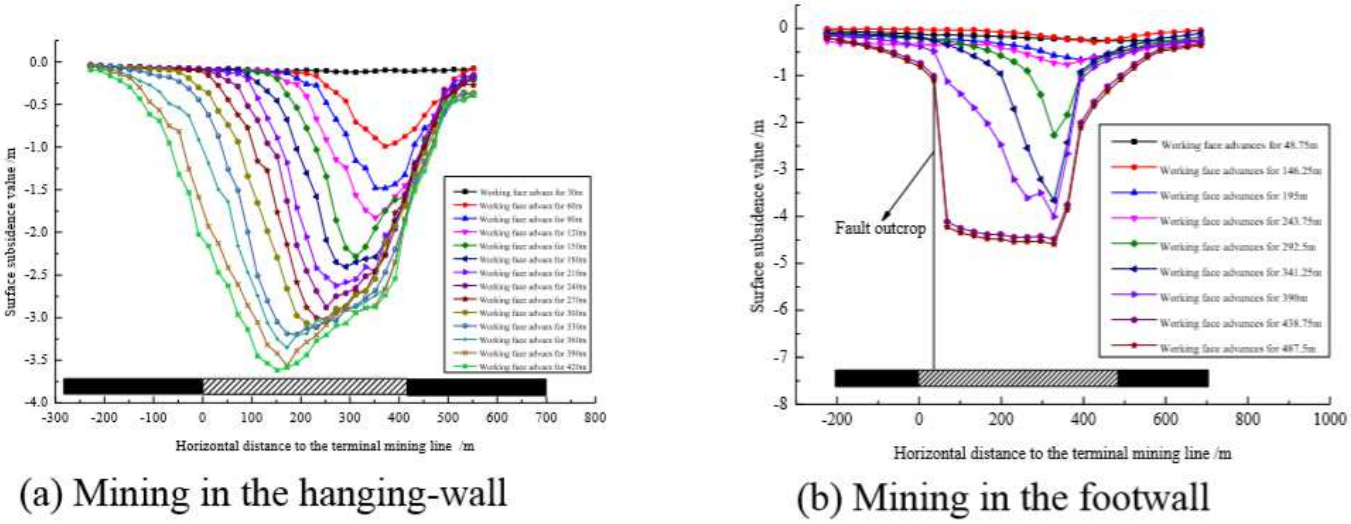

(a) Mining in the hanging-wall

(b) Mining in the footwall

Figure 14

Surface subsidence profiles when advancing the working face

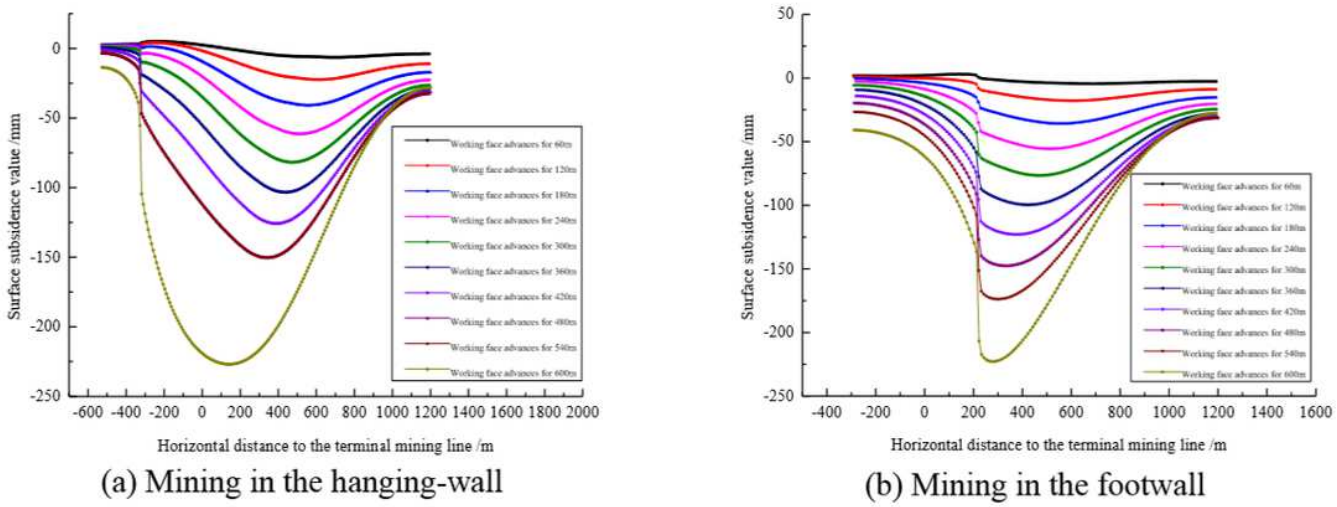

Figure 14

Surface subsidence when advancing the working face to a fault

(a) Mining in the hanging-wall

(b) Mining in the footwall

Figure 14

Fractures in the surface at fault outcrop when mining is finished

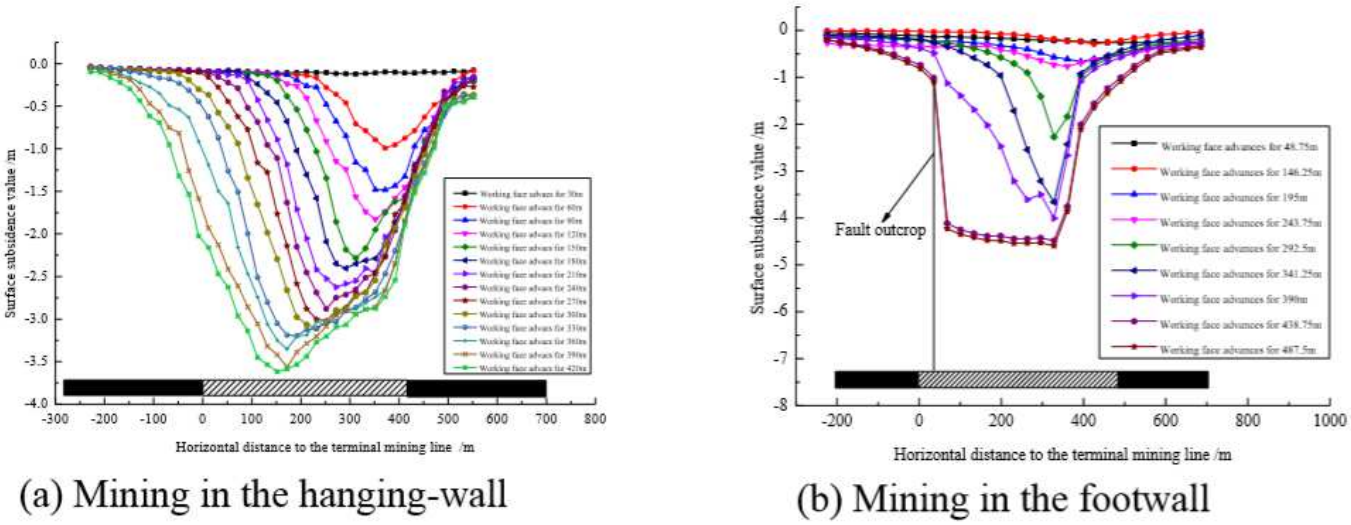

(a) Mining in the hanging-wall

(b) Mining in the footwall

Figure 14

Surface subsidence profiles when advancing the working face

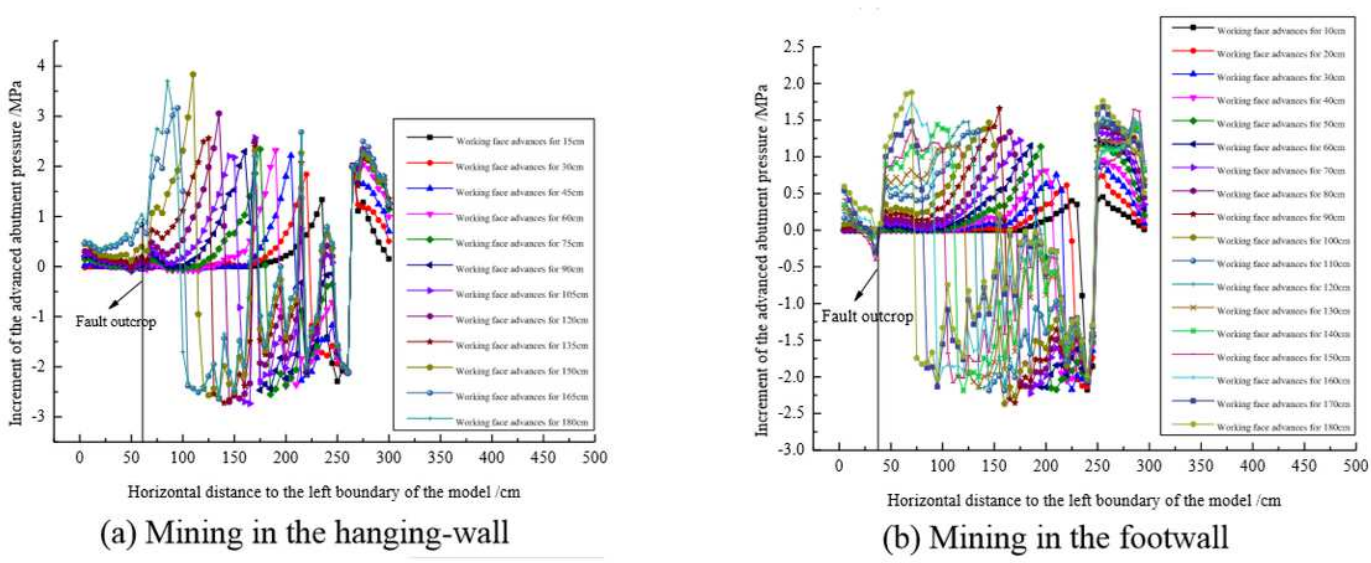

(a) Mining in the hanging-wall

(b) Mining in the footwall

Figure 15

Changes in advanced abutment pressure when the working face advances to a fault

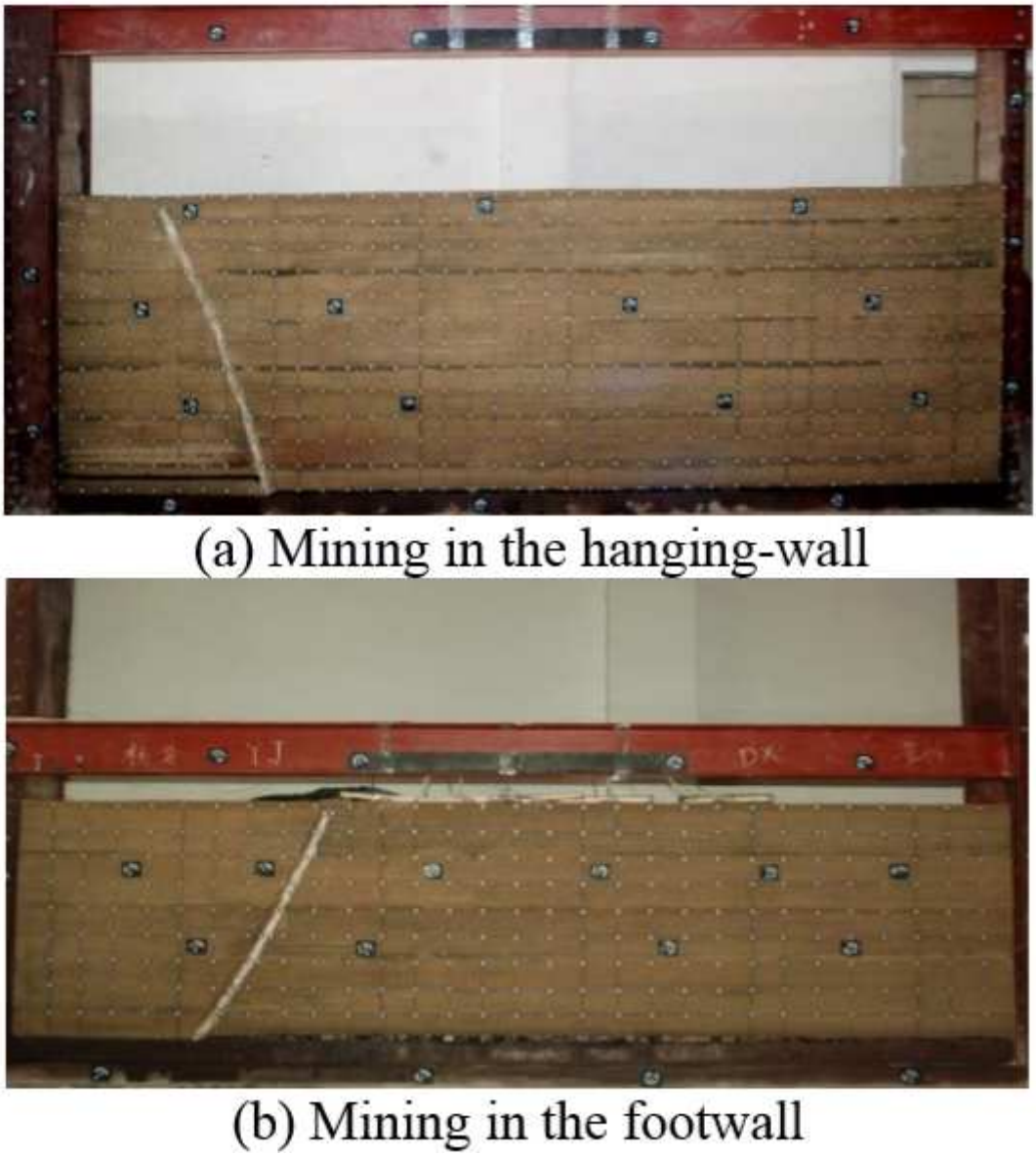

(a) Mining in the hanging-wall

(b) Mining in the footwall

Figure 15

Similarity models when mining in the hanging wall and footwall

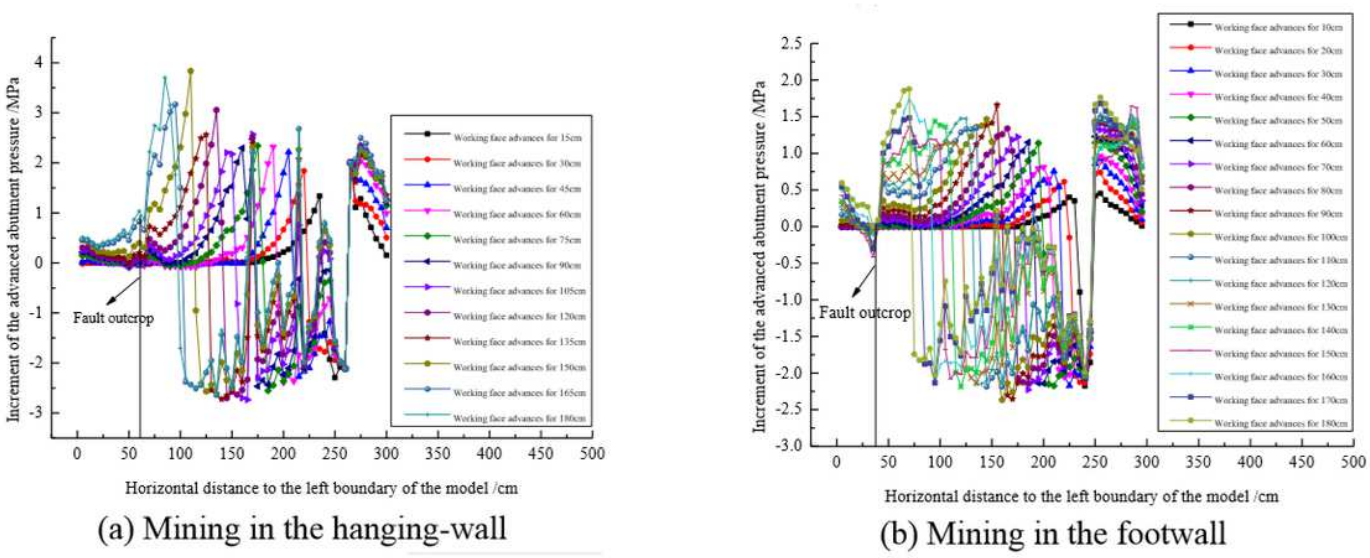

Figure 15

Changes in advanced abutment pressure when the working face advances to a fault

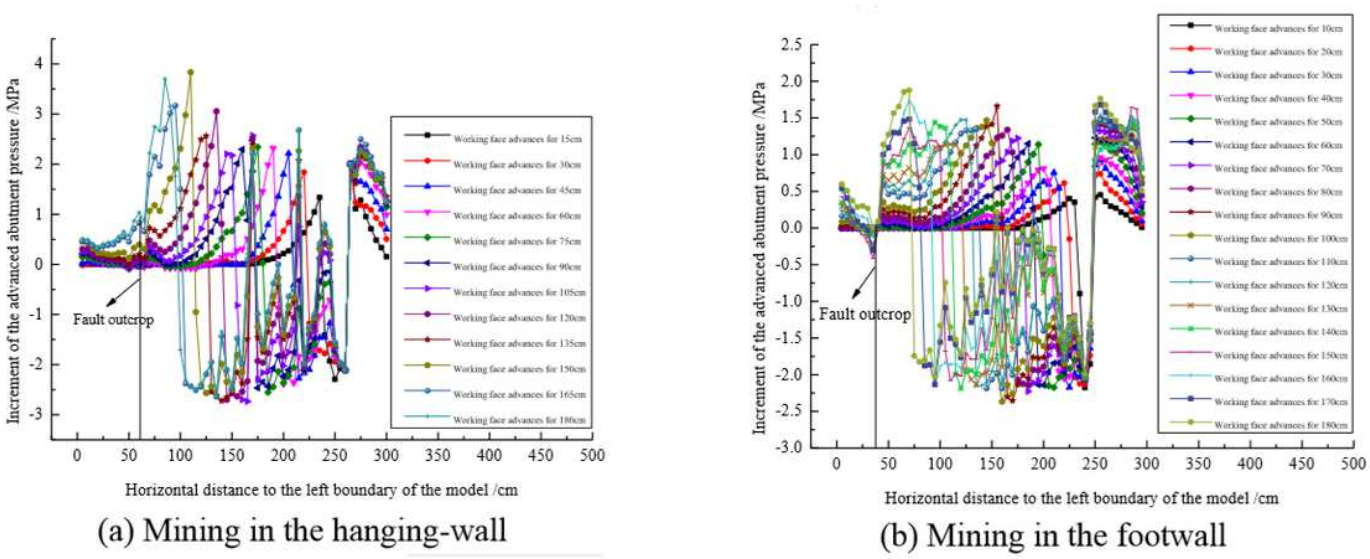

Figure 15

Changes in advanced abutment pressure when the working face advances to a fault

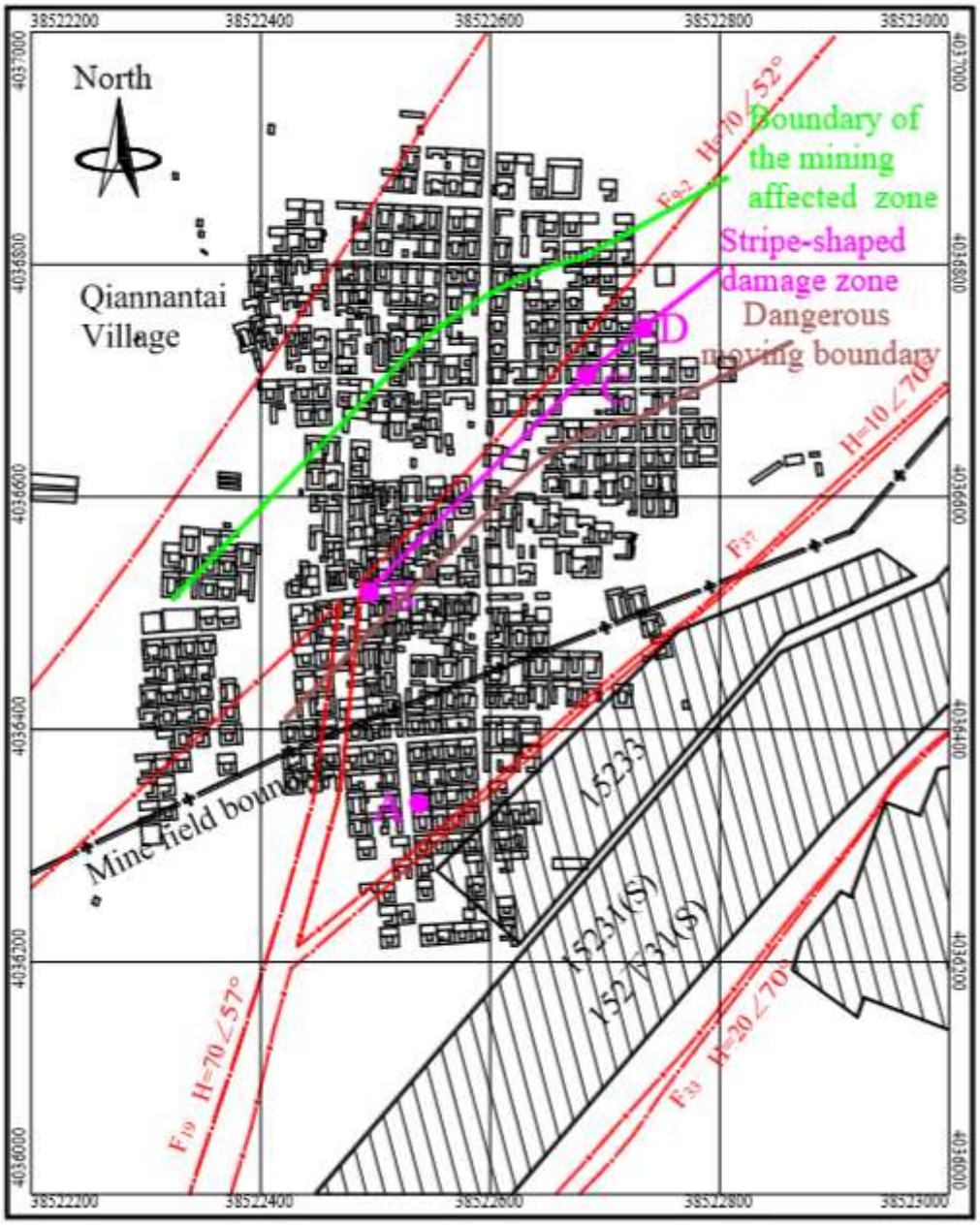

Figure 16

The boundary of the zone affected by mining and the dangerous moving boundary

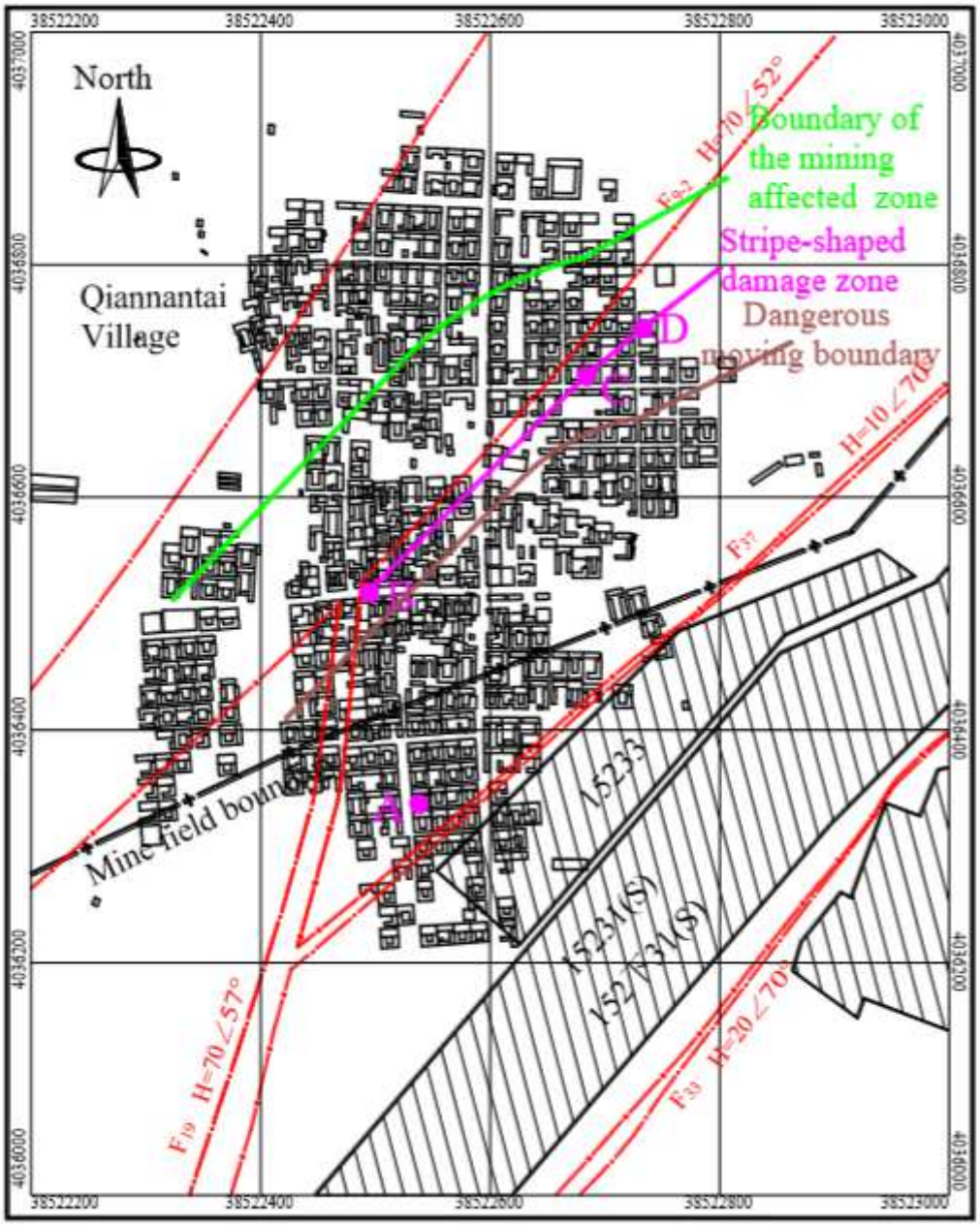

Figure 16

The boundary of the zone affected by mining and the dangerous moving boundary

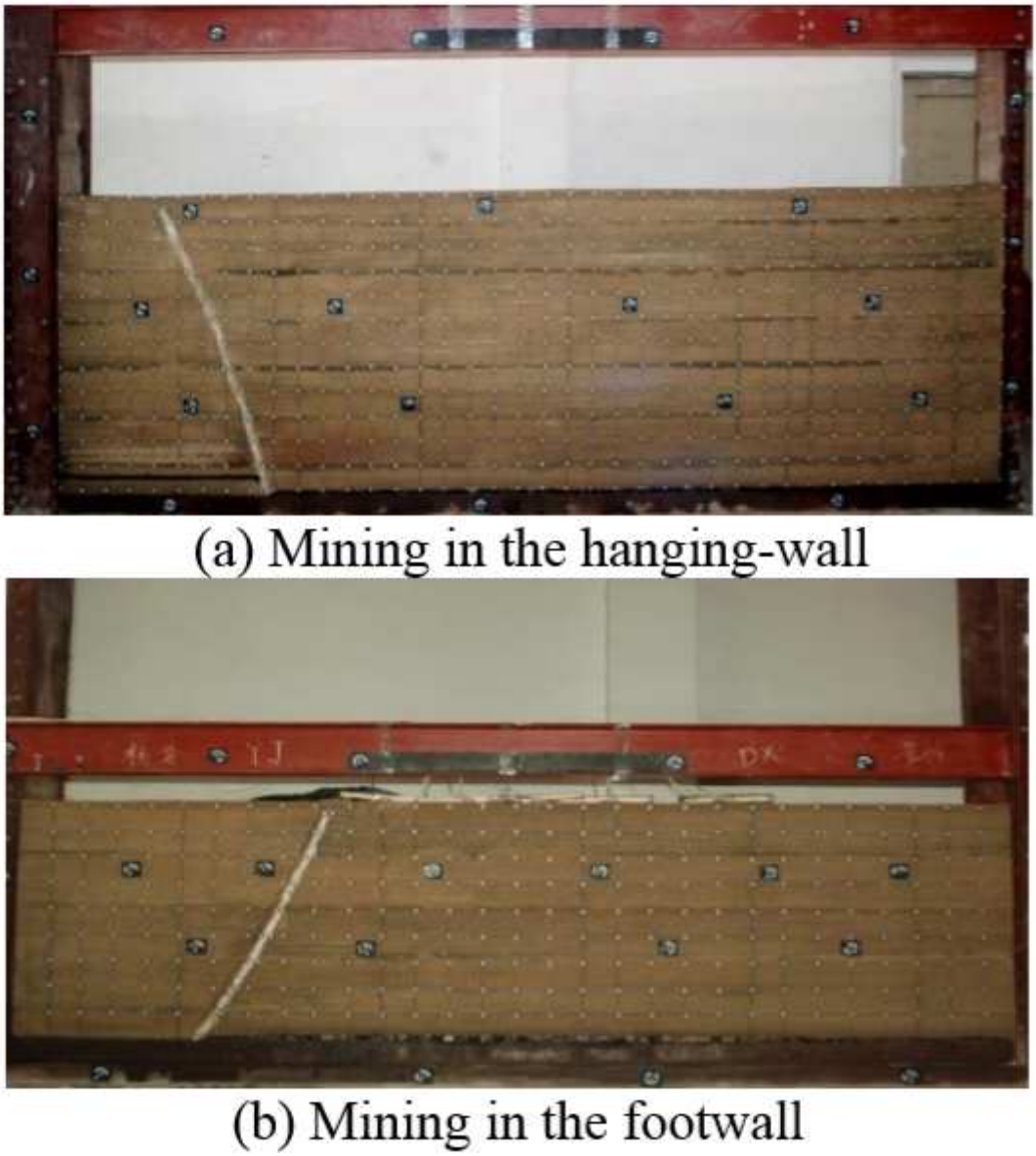

Figure 16

Similarity models when mining in the hanging wall and footwall

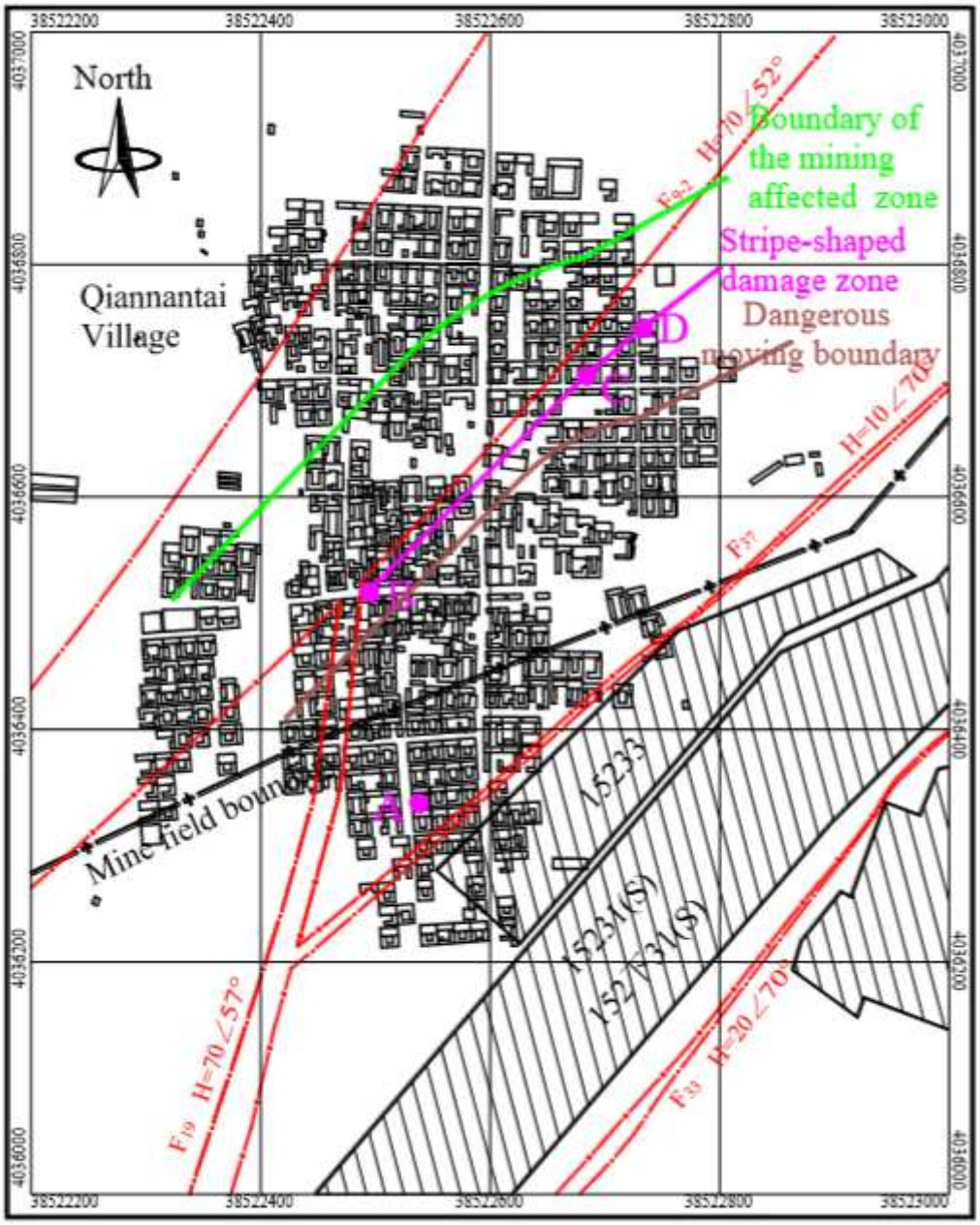

Figure 16

The boundary of the zone affected by mining and the dangerous moving boundary

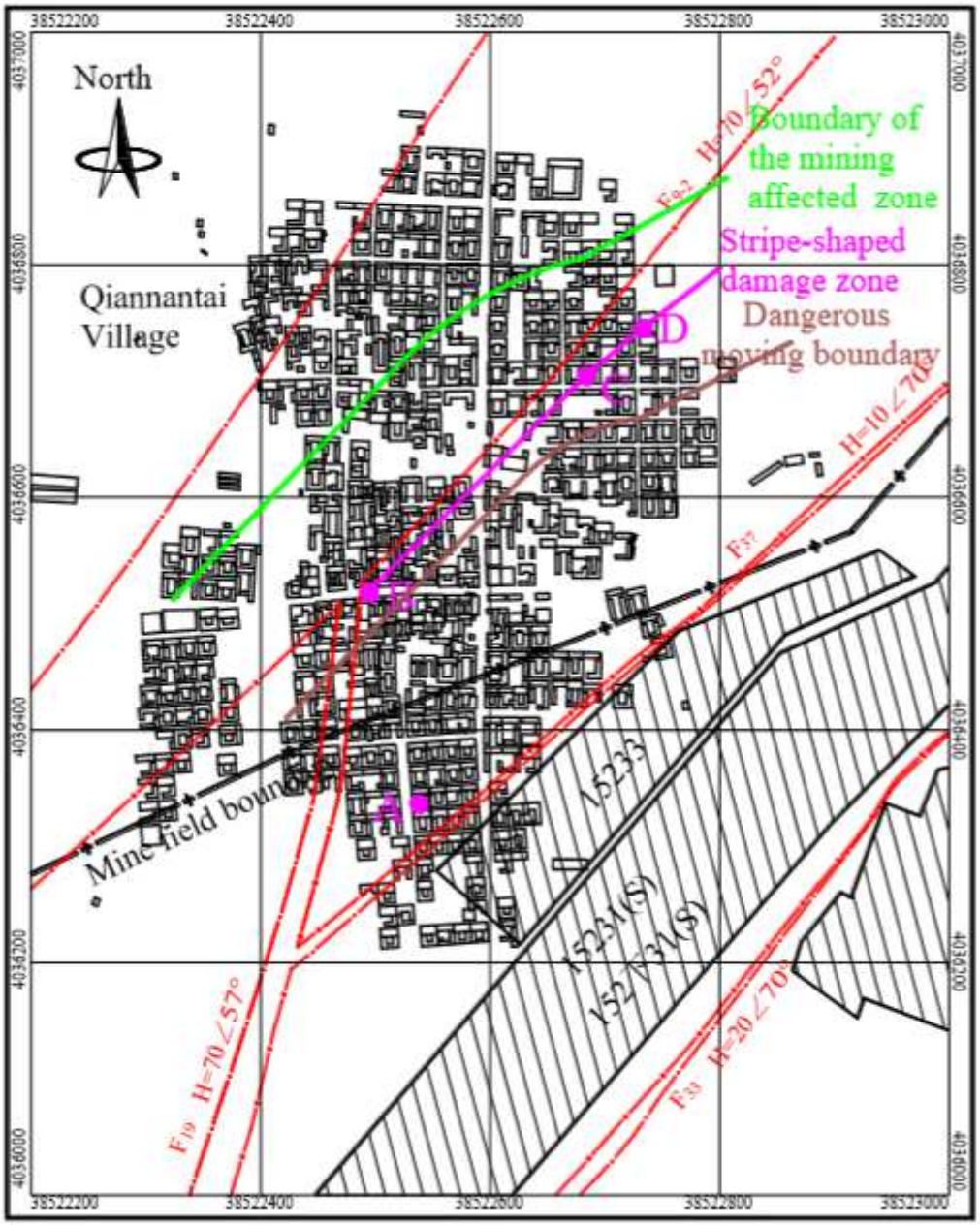

Figure 16

The boundary of the zone affected by mining and the dangerous moving boundary

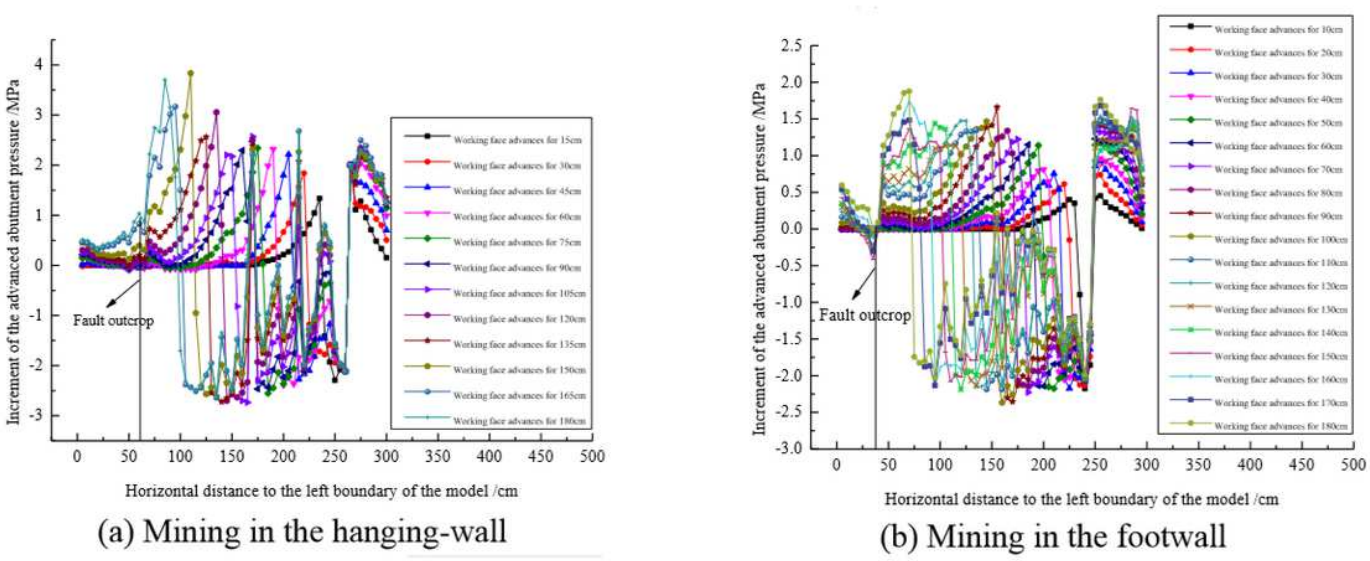

Figure 16

Changes in advanced abutment pressure when the working face advances to a fault

Figure 17

Damage to buildings at the fault outcrop

Figure 17

Damage to buildings at the fault outcrop

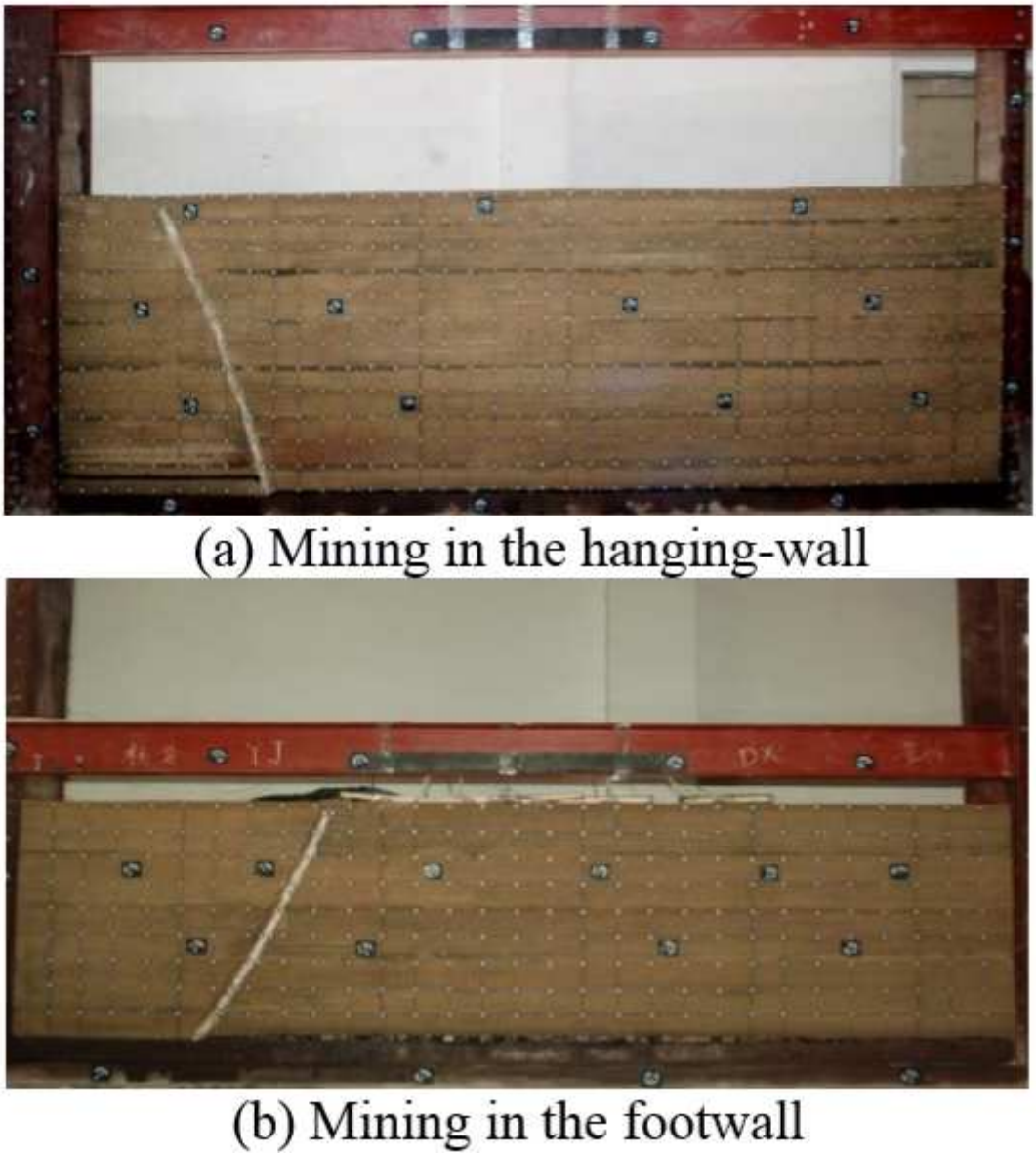

Figure 17

Similarity models when mining in the hanging wall and footwall

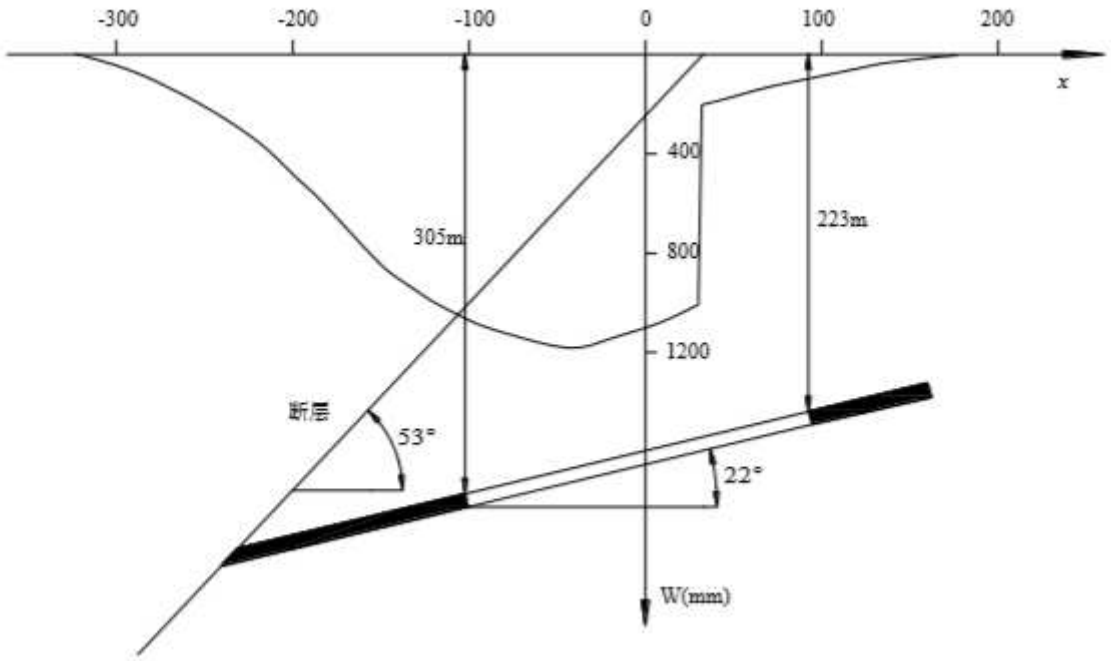

Figure 18

Surface subsidence profile of the main inclined section in Qinghemen Mine

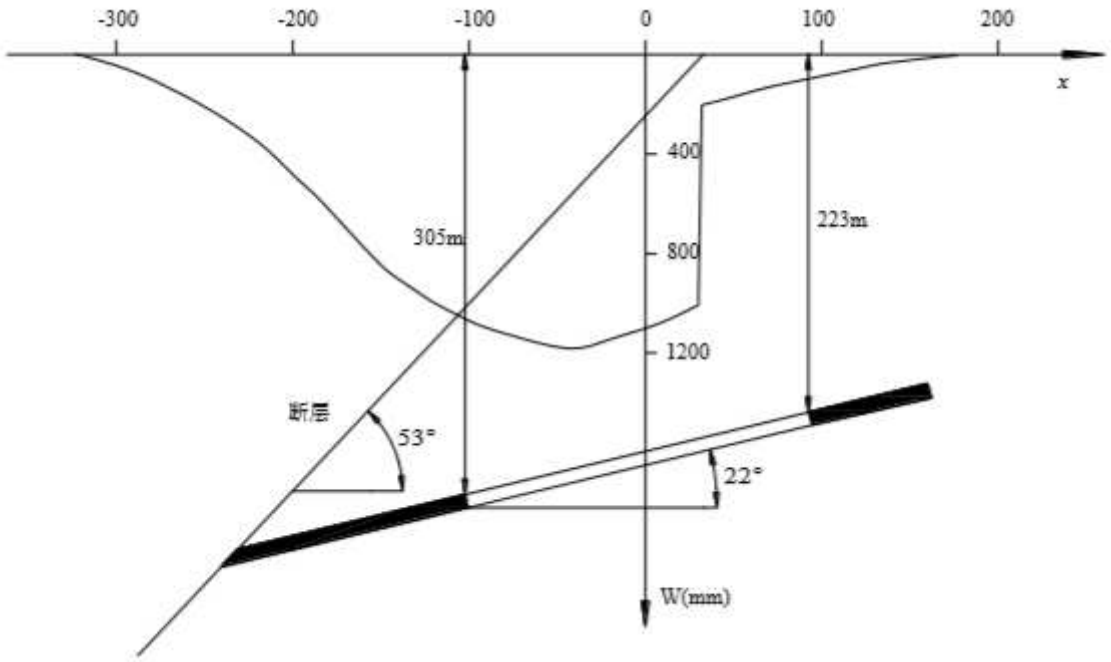

Figure 18

Surface subsidence profile of the main inclined section in Qinghemen Mine

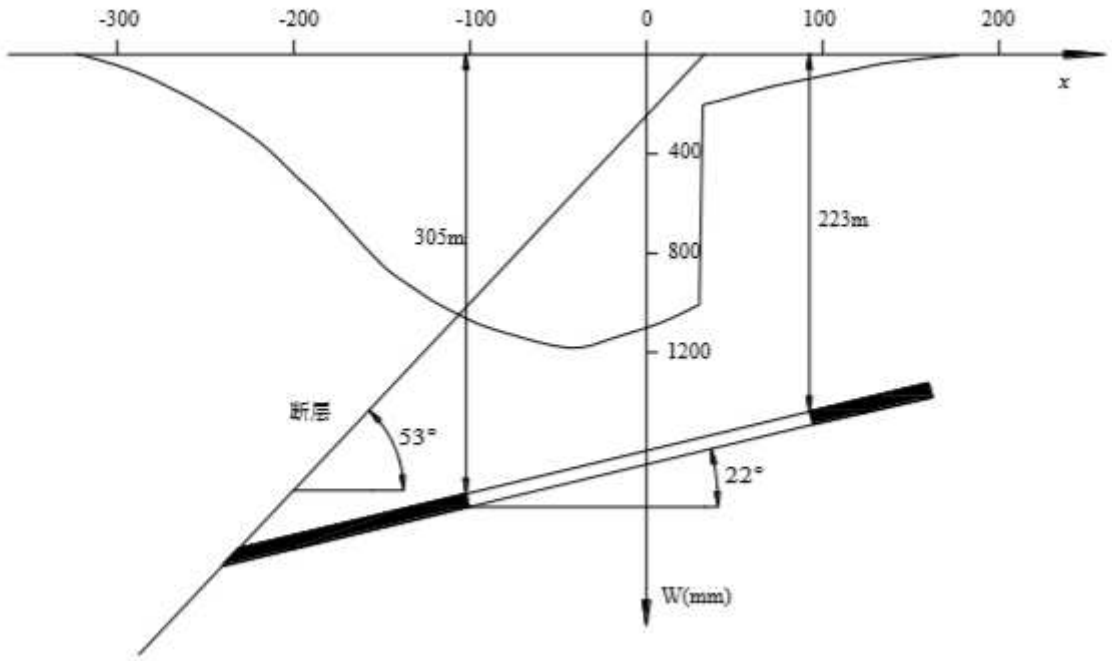

Figure 18

Surface subsidence profile of the main inclined section in Qinghemen Mine

Figure 18

Damage to buildings at the fault outcrop

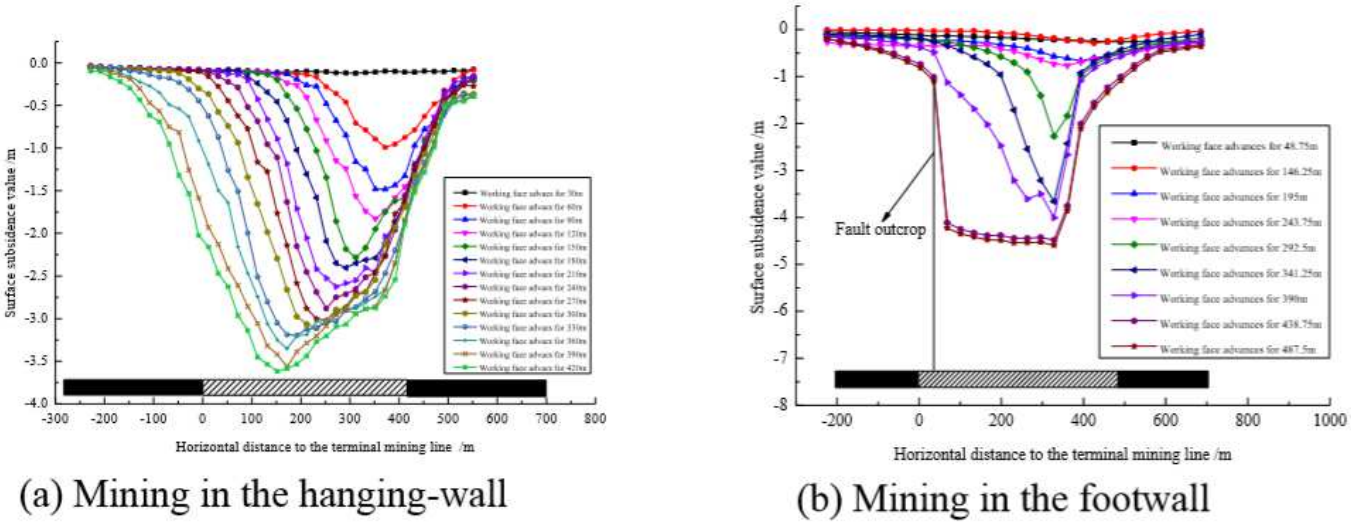

Figure 20

Surface subsidence profiles when advancing the working face

Figure 23

Damage to buildings at the fault outcrop